JACS
JOURNAL OF THE AMERICAN CHEMICAL SOCIETY
Article
pubs.acs.org/JACS

Mechanism of Cu/Pd-Catalyzed Decarboxylative Cross-Couplings: A DFT Investigation

Andreas Fromm, Christoph van Wüllen, Dagmar Hackenberger, and Lukas J. Gooßen*

Fachbereich Chemie and Forschungszentrum OPTIMAS, TU Kaiserslautern, Erwin-Schrödinger-Straße, 67663 Kaiserslautern, Germany

Supporting Information

ABSTRACT: The reaction mechanism of decarboxylative cross-couplings of benzoates with aryl halides to give biaryls, which is cooperatively catalyzed by copper/palladium systems, was investigated with DFT methods. The geometries and energies of all starting materials, products, intermediates, and transition states of the catalytic cycle were calculated for the two model reactions of potassium 2- and 4-fluorobenzoate with bromobenzene in the presence of a catalyst system consisting of copper(I)/1,10-phenanthroline and the anionic monophosphine palladium complex $[Pd(PMe_3)Br]^-$. Several neutral and anionic pathways were compared, and a reasonable catalytic cycle was identified. The key finding is that the transmetalation has a comparably high barrier as the decarboxylation, which was previously believed to be solely rate-determining. The electronic activation energy of the transmetalation is rather reasonable, but the free energy loss in the initial Cu/Pd adduct formation is high. These results suggested that research aimed at further improving the catalyst should target potentially bridging bidentate ligands likely to assist in the formation of bimetallic intermediates. Experimental studies confirm this somewhat counterintuitive prediction. With a bidentate, potentially bridging ligand, designed to support the formation of bimetallic adducts, the reaction temperature for decarboxylative couplings was reduced by 70 °C to only 100 °C.

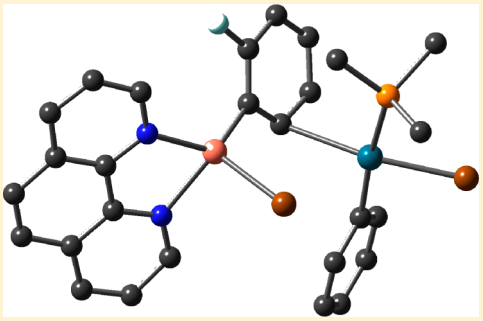

INTRODUCTION

Decarboxylative couplings have become a powerful tool for the selective formation of carbon−carbon and carbon−heteroatom bonds. In these transformations, CO_2 is extruded from a carboxylic acid precursor, and the carbon atom that has carried the carboxylic group then forms a bond with an electrophilic carbon or heteroatom. Following pioneering contributions by Nilsson, Tsuji, and Myers,[1] a redox-neutral decarboxylative biaryl synthesis was discovered in 2006 in which aromatic carboxylic acids are coupled with various aryl bromides in the presence of a copper/palladium bimetallic catalyst system (Scheme 1).[2]

Scheme 1. Decarboxylative Coupling Reactions

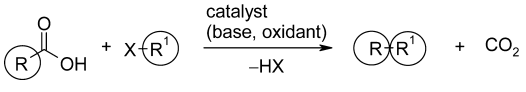

Since then, bimetallic systems have been used for decarboxylative couplings of benzoates and α-imino-[3] and α-oxocarboxylates[4] with aryl iodides, bromides,[5] chlorides,[6] triflates,[7] tosylates,[8] and mesylates.[9] Decarboxylative couplings with monometallic catalysts include Cu-mediated arylations of perfluorinated arenecarboxylic acids,[10] Rh-catalyzed decarboxylative 1,2-additions,[11] Pd-catalyzed decarboxylative allylations[12] and arylations of five-ring heteroarene carboxylates,[13] of alkynylcarboxylates,[14] and of oxalic acid monoesters,[15] and Mannich-type reactions.[16] Oxidative decarboxylative cross-couplings have been used for Heck-type vinylations,[1f−h,17] C−H arylations,[18] couplings of amino acids,[19] and various C−heteroatom bond formations.[20]

The concept of decarboxylative couplings has distinct advantages over traditional cross-coupling reactions in the regiospecific formation of C−C bonds, because it relies on inexpensive and broadly available carboxylate salts instead of expensive and sensitive preformed organometallic reagents as the source of carbon nucleophiles.

Typical catalyst systems and the reaction scope are shown in Scheme 2.

Especially in redox-neutral couplings of aromatic carboxylate salts, bimetallic copper/palladium systems have proven to be the most generally applicable catalysts. For these systems, a mechanistic outline consisting of two interlinked catalytic cycles has been proposed (Scheme 3).[2,5] The ligand environment at the copper center is designed to promote the extrusion of CO_2 with the highest possible efficiency, while the palladium catalyst is independently optimized for the cross-coupling step. The proposed catalytic cycle starts with an anion exchange at the copper center, in the course of which the aromatic carboxylate is transferred to the copper complex **a** to give the metal carboxylate **b**. In the decarboxylation step, an organocopper

Received: April 2, 2014
Published: June 26, 2014

   dx.doi.org/10.1021/ja503295x | J. Am. Chem. Soc. 2014, 136, 10007−10023

Scheme 2. Representative Decarboxylative Cross-Couplings with Bimetallic Cu/Pd Catalyst Systems[a]

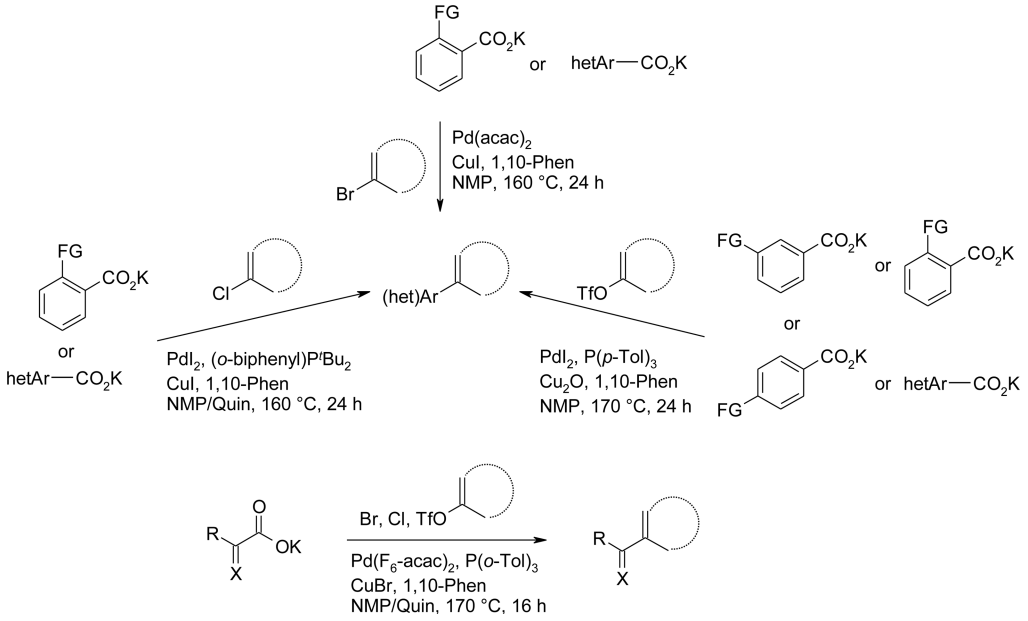

[a]Ar = aryl, FG = functional group, hetAr = heteroaryl, Phen = phenanthroline, Quin = quinoline, X = O, NR.

Scheme 3. Mechanism Proposed for Decarboxylative Cross-Couplings

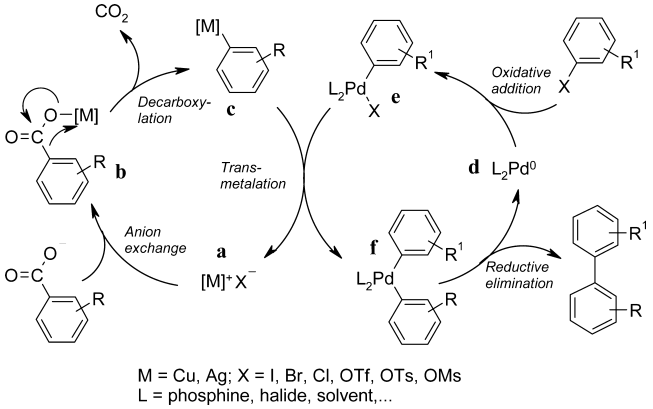

species **c** is generated by extrusion of CO_2. A subsequent transmetalation links the two catalytic cycles. In this step, an aryl residue is transferred from the copper species **c** onto a palladium species **e** that has been generated by oxidative addition of the aryl electrophile to a low-valent palladium(0) cocatalyst **d**, and the original copper species **a** is regenerated. The resulting diaryl palladium species **f** undergoes reductive elimination, in which the new carbon−carbon bond is formed, the biaryl product is released, and the palladium(0) species **d** is regenerated.

At present, most decarboxylative couplings still require temperatures in excess of 160 °C, which, in practice, represents the main limitation of this elegant reaction type. The rational development of catalysts that promote decarboxylative couplings at lower temperatures is, thus, in the focus of current research activities. In this context, mechanistic investigations and theoretical studies are of vital importance.[21]

However, DFT modeling of the mechanistically complex decarboxylative couplings catalyzed by bimetallic systems poses a considerable challenge, which has so far precluded the calculation even of simplified models. Computational studies of this reaction have to date been limited to the decarboxylation step (**b** → **c** in Scheme 3).[22] That this step was rate-determining in the early reaction protocols became evident from the observation that Cu-catalyzed protodecarboxylations required temperatures that were at least as high as those of decarboxylative cross-couplings (170 °C). In contrast, Pd-mediated cross-couplings of aryl−copper species are known to proceed at much lower temperatures.

These DFT calculations confirmed[22] that the extrusion of CO_2 from phenanthroline copper benzoates is endothermic by 9.9−28.8 kcal mol^{-1} and endergonic (0.8−17.5 kcal mol^{-1}) and has a considerable activation barrier of 27.2−36.1 kcal mol^{-1}.[21c] Another correct prediction derived from these calculations was that for a narrow range of substitution patterns, e.g. *o*-methoxybenzoates, the energy barrier for the decarboxylation is substantially lower when copper is replaced by silver, whereas the majority of carboxylates lose CO_2 more easily when coordinated to copper rather than silver complexes.[7c]

Pd-catalyzed cross-couplings of organometallic reagents have been intensively studied by DFT calculations.[23] For Suzuki-type couplings of carboxylic anhydrides with arylboronic acids, various catalytic cycles were computed starting from neutral $(PMe_3)_2Pd(0)$ (**4**), anionic tricoordinate Amatore−Jutand-type $[(PMe_3)_2Pd(0)OAc]^-$ (**5**), and anionic dicoordinate $[(PMe_3)$-$PdOAc]^-$ (**6**) (Figure 1).[24] With the anionic dicoordinate palladium complex **6**, the energy profile obtained was most favorable overall so that this species appears to be the optimal candidate for calculations of related Pd-catalyzed couplings.

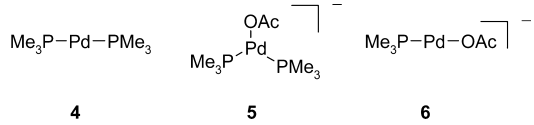

Figure 1. Pd-species investigated in Suzuki-type cross-couplings.

dx.doi.org/10.1021/ja503295x | J. Am. Chem. Soc. 2014, 136, 10007−10023

Scheme 4. DFT Investigations of Decarboxylative Cross-Couplings with Monometallic Catalysts

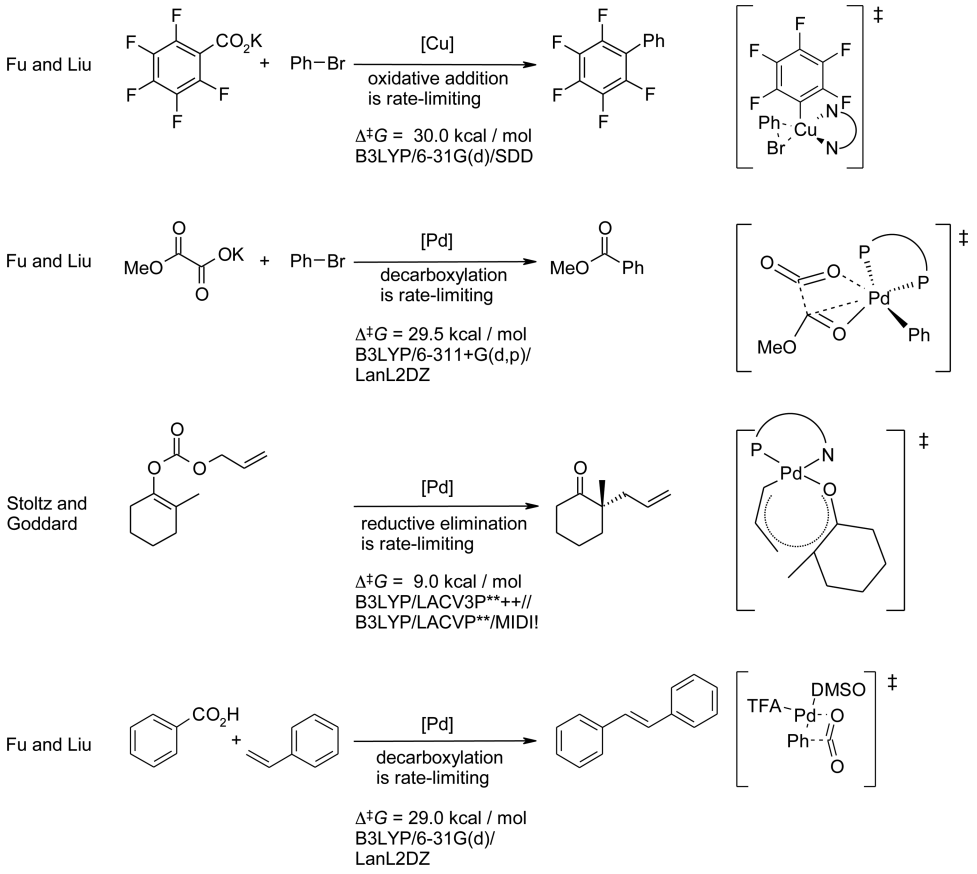

Scheme 5. Model Reactions of Potassium 2- and 4-Fluorobenzoate with Bromobenzene

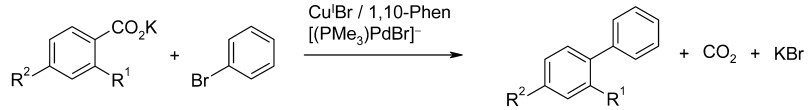

7a: R^1 = F, R^2 = H
7b: R^1 = H, R^2 = F

8

9a: R^1 = F, R^2 = H
9b: R^1 = H, R^2 = F

3

10

As mentioned above, some particularly activated substrates can be decarboxylatively coupled with aryl electrophiles by using monometallic catalysts. The reduced complexity of such monometallic systems has permitted in-depth mechanistic investigations (see Scheme 4). DFT studies were reported for Pd-catalyzed decarboxylative cross-couplings of oxalic acid monoesters,[15] decarboxylative allylations of enol carbonates,[12,25] decarboxylative cross-couplings of polyfluorobenzoates with aryl electrophiles,[26] Myers' Pd-catalyzed decarboxylative Heck vinylation,[17a] and certain intramolecular decarboxylative couplings.[27]

For the mechanistically more complex decarboxylative couplings mediated by bimetallic catalyst systems, a similarly detailed computational study would be of substantial value. With state-of-the-art catalysts, the protodecarboxylation of *o*-nitrobenzoic acids with a copper/phenanthroline system can meanwhile be performed at 100 °C,[28] while decarboxylative cross-couplings with aryl triflates, in which copper/phenanthroline systems are employed as the decarboxylation cocatalysts, still do not proceed below 150 °C.[7a,b] Thus, the decarboxylation is not necessarily rate-determining, and it is no longer sufficient to single out the decarboxylation step in computational studies to obtain a lead for further catalyst optimization. Instead, computational modeling should cover the entire catalytic cycle. A particular challenge lies in modeling the transmetalation step, in which an organic residue is transferred from a fully ligated copper complex to a phosphine-stabilized arylpalladium species.[29]

■ MODEL SYSTEM

We herein investigate the decarboxylative coupling of bromobenzene (**8**) with (a) potassium 2-fluorobenzoate (**7a**) as an example of a highly reactive arenecarboxylate and (b) potassium 4-fluorobenzoate (**7b**) as an example of an arenecarboxylate with low reactivity (Scheme 5).

The catalyst system employed in the calculations of these representative model reactions is composed of 1,10-phenanthroline copper(I) bromide, which is known to display a substantially greater decarboxylation activity than simple copper(I) salts,[2] and an anionic Pd(0) bromide catalyst with the simplified but still reasonably realistic ligand PMe_3.

Comparative studies performed upfront, in combination with related literature studies, confirmed that the catalytic cycle

dx.doi.org/10.1021/ja503295x | J. Am. Chem. Soc. 2014, 136, 10007−10023

Scheme 6. Catalytic Cycles Calculated for Decarboxylative Cross-Couplings

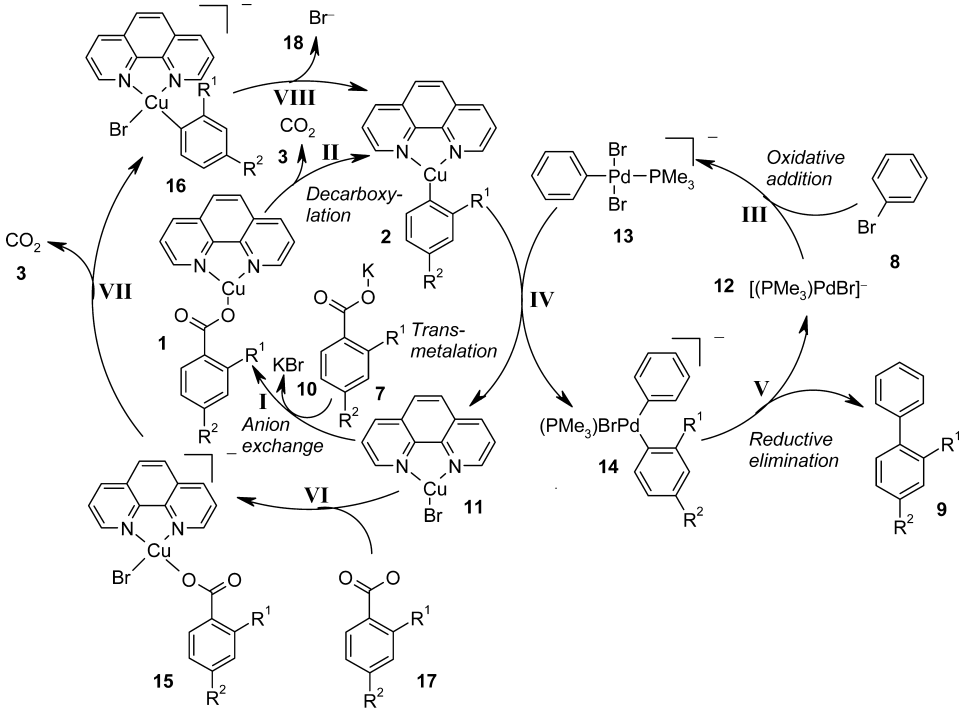

shown in Scheme 6 is a realistic mechanistic model. For example, computational studies of Suzuki-type couplings led to the conclusion that catalytic cycles starting from various Pd(0) species, each of which may be present in solution, will have comparable energy profiles also in couplings with other carbon nucleophiles.[24] Among them, a pathway starting from $[(PMe_3)PdOAc]^-$ (**6**) (Figure 1) had proven to be the most advantageous overall. It thus appeared to be reasonable to use an analogous cycle based on similar structural units as a starting point for computing the cycle of the Pd-catalyst in the decarboxylative cross-coupling. For the Cu-catalyst, two different catalytic cycles were computed, both starting from 1,10-phenanthroline copper(I) bromide. The first solely involves neutral species, whereas in the second, an additional bromide is bound to copper during the decarboxylation step. This was calculated to find a possible explanation for the profound influence of bromide ions on the decarboxylation of non-*ortho*-substituted benzoates.

Both variants of the catalyst cycle were successfully calculated. Minima with reasonable structures and energies could be found for all intermediates, and transition states connecting these intermediates could be located. The computational studies led us to conclude that decarboxylative cross-couplings follow a neutral pathway consisting of the anion exchange (step I) and the decarboxylation step (step II) at the copper catalyst, the oxidative addition (step III) of the bromobenzene to the Pd catalyst, the transmetalation process (step IV) between the resulting palladium and copper species, and the reductive elimination (step V) of the biaryl product with regeneration of the Pd catalyst. Subsequently, the computational study of an anionic variant of the Cu-cycle is presented, which starts with the coordination (step VI) of the carboxylate to the copper catalyst, followed by decarboxylation (step VII) and bromide decoordination (step VIII). This alternative cycle was found to be less favorable.

COMPUTATIONAL METHOD

All calculations were performed with use of the Gaussian 03 or Gaussian 09 software packages.[30] The B3LYP exchange-correlation functional[31] was used in all cases. For the geometry optimizations, the polarized split-valence 6-31+G(d) basis set[32] was employed for all atoms except Cu and Pd, where a scalar-relativistic effective core potential[33] replaced 10 (Cu) or 28 (Pd) core electrons, together with the valence basis sets[33] in double-ζ quality. Spherical basis functions (5D, 7F) were used in all cases. In contrast to our previous studies,[21c,22] some of the species investigated are anionic, so that diffuse basis functions were included in the basis set. Note that the valence basis sets for Cu and Pd already contain diffuse functions from the outset.

All geometries of minima (intermediates) and transition states were fully optimized for isolated (gas-phase) molecules. To locate the transition states, we first performed a relaxed potential energy surface scan in which the reaction coordinate was kept fixed at several defined distances, while all other degrees of freedom were optimized. In these scans, a series of structures were optimized in which the reaction coordinate was increased stepwise. The structure with the highest energy was then used as a starting point for the synchronous transit-guided quasi-Newton method[34] to locate the transition state with a molecular Hessian of exactly one negative eigenvalue. To identify the minima connected to the transition states thus identified, the intrinsic reaction coordinate (IRC)[35] was followed downhill for 10 points in both directions and the two resulting molecular geometries were used as starting points for subsequent geometry optimizations. Sometimes, additional intermediates were discovered this way. In these cases, the process described above was repeated until the reaction pathway was complete. For each molecular structure (intermediate or transition state), the calculated electronic energy (but not the molecular structure and harmonic vibrational frequencies) was improved by a single-point calculation in which the 6-31+G(d) basis (for all atoms except Cu and Pd) was replaced by the better polarized valence triple-ζ type 6-311+G(2d,p).[36] For Cu and Pd, the *d* functions of the original basis sets were decontracted slightly from [411] to [3111], and a single set of *f* functions (taken from the def2-TZVP basis sets,[37] η_f(Cu) = 2.233, η_f(Pd) = 1.24629) was added for both elements.

The above calculations provided electronic energies under vacuum (E_{tot}). To model the reaction energies more closely resembling

dx.doi.org/10.1021/ja503295x | J. Am. Chem. Soc. 2014, 136, 10007−10023

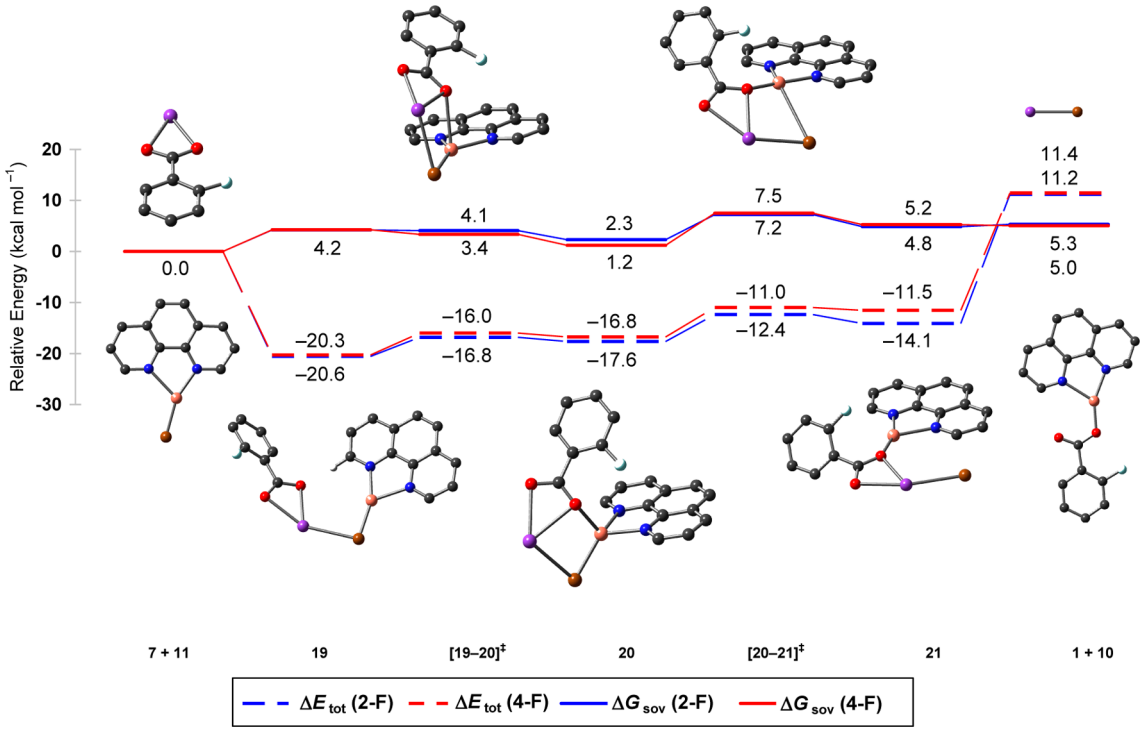

Figure 2. B3LYP/6-31+G(d) optimized structures for the anion exchange of potassium 2-fluorobenzoate and phenanthroline copper(I) bromide; hydrogens are omitted for clarity. Energy and solution Gibbs energy profiles overlaid for 2- and 4-fluorobenzoate. Color code: C, black; H, white; Br, brown; Cu, orange; F, turquoise; K, purple; N, blue; O, red.

experimental conditions, further terms were added, namely zero-point vibrational energy, thermal corrections to the energy, solvation and entropic effects, as well as empirical dispersion corrections. This way, an approximation to the Gibbs energy in solution (G_{sov}) was obtained.

Solvent effects were included by estimating the Gibbs energy of solvation for all intermediates and transition states using the conductor-like polarizable continuum model[38] (CPCM) of Gaussian 09, which is an implementation of the conductor-like screening solvation model[39] (COSMO). This model is particularly well-suited for polar solvents such as *N*-methyl-2-pyrrolidone (NMP, ε = 32.55), which is the most effective solvent for decarboxylative cross-couplings.

To calculate the zero-point vibrational energies, the harmonic frequencies calculated (with the small basis) were scaled by a factor of 0.9613 as suggested by Wong.[40] The thermal correction to the Gibbs energy of each component depends on its concentration in the solution. Note that in the Gaussian program one has to specify the concentration as a pressure value, using the ideal gas law $p_i = RTn_i/V$, where p_i is the pressure, R the gas constant, T the absolute temperature, n_i the molar quantity, and V the reaction volume. Typical experiments, as modeled in our calculations, involve approximately 1 mmol of starting material and product in a reaction volume of 2 mL, which corresponds to a pressure of 1,844,115 Pa (18.2 atm) at a reaction temperature of 443 K. The amount of catalyst is lower by a factor of 20, so that we used a pressure of 101,325 Pa (1 atm) for all species involving Cu and/or Pd. The experimental solubility data of CO_2 in NMP[41] show that under the experimental conditions, the molar fraction of CO_2/NMP is clearly less than 0.01, most likely about 0.001 when extrapolating temperature and pressure, which implies that most of the CO_2 leaves the NMP solution. The resulting CO_2 concentration in the reaction mixture corresponds to a partial pressure of 101,325 Pa (1 atm) for an ideal gas. Because of the ideal gas approximation, the molar Gibbs energy for a given temperature T and pressure p was computed from the results for p_0 = 1 atm as $G(T,p) = G(T,p_0) + RT \ln(p/p_0)$.

For any sequence of elementary steps that involve a single species, the reaction profile does not depend on the concentration. This changes if association and dissociation steps are involved. These considerations are relevant in this context because we have two coupled catalytic cycles. Reducing the catalyst load (both Cu and Pd) reduces the reaction rate of the steps involving only Cu or only Pd linearly, while the transmetalation step is affected quadratically. Therefore, the relative rates of the transmetalation compared to the other elementary steps depend on the catalyst load, with lower loads disfavoring the transmetalation. This is taken into account in our Gibbs energy profiles.

It is known that standard DFT methods neglect or severely underestimate London dispersion interactions.[42] A robust and numerically inexpensive way to cure this deficiency is to add an empirical dispersion correction that sums up the contribution of all atom pairs. We used Grimme's D3 parametrization[43] and calculated the dispersion correction for all minima and transition states. These values are included in our final solution Gibbs energies G_{sov}. This correction significantly lowers the Gibbs energy of an encounter complex with respect to the two fragments, but also lowers the Gibbs energy of a tight transition state with respect to a loose intermediate.

Note that the solvation model as used in our calculations does not include nonelectrostatic solute−solvent interactions: in a numerical experiment, we found zero contributions when we set the dielectric constant to zero. This means that the loss of solute−solvent dispersion interaction upon formation of an adduct, which is a consequence of reducing the surface of the solute(s), is not taken into account. Therefore, we think that the dispersion interaction in solution is somewhat overestimated in our calcualtions, although the combination of empirical dispersion and solvent corrections has been reported to work well.[44]

In the Supporting Information, the electronic energies (with and without solvation), the calculated Gibbs energies at 298 and 443 K (at 1 and 18.2 atm), the empirical dispersion corrections, and the final solution Gibbs energy including empirical dispersion corrections G_{sov} are documented. The diagrams in this paper contain the electronic energy E_{tot} (since molecular geometries and vibrational frequencies are obtained at this level) and solution Gibbs energy G_{sov} profiles including empirical dispersion corrections (which govern the reactivity). Throughout the text, all bond lengths are given in Å and

dx.doi.org/10.1021/ja503295x | J. Am. Chem. Soc. 2014, 136, 10007−10023

relative energies are expressed in kcal mol^{-1}. All ball-and-stick models are rendered with GaussView 5.[45]

MODELING THE CATALYTIC CYCLE BY DFT

Anion Exchange. In the anion exchange step, the potassium benzoate (**7a**/**b**) reacts with the phenanthroline copper bromide catalyst **11** to afford the corresponding phenanthroline copper benzoate (**1a**/**b**) along with potassium bromide (**10**). The energy and solution Gibbs energy profiles for the model substrates, 2- and 4-fluorobenzoate are depicted in Figure 2, along with the optimized structures for the *o*-fluoro derivates.

The anion exchange starts with the formation of an encounter complex **19** between the substrates **7** and **11**. This process is exothermic in the gas phase (Δ_rE_{tot} = −20.6 kcal mol^{-1}) but endergonic by Δ_rG_{sov} = 4.2 kcal mol^{-1}. This difference has two origins. First, entropy is lost when forming the adduct, even more so because the copper catalyst **11** is present only in low concentration compared to the substrate **7**. This entropy loss strongly contributes to the increase in Gibbs energy at the elevated reaction temperature (170 °C). Second, solvation disfavors adduct formation, since the combined solvation energies for **7** and **11** are larger than that for the adduct **19**. In the adduct, the C(2)−H bond of the 1,10-phenanthroline points toward one of the carboxylate oxygens, resulting in a short C−H···O (2.03 Å) and a long K−Br distance (3.26 Å). A Cu−O bond has not formed at this stage. The K−O bond is slightly elongated to 2.64 Å compared to 2.55 Å in **7**. Also, the Cu−Br bond is slightly increased to 2.30 Å compared to 2.26 Å in **11**.

Bringing a carboxylic oxygen closer to the copper center leads to the transition state [**19**−**20**]‡. This process has a very small barrier ($\Delta^{‡}E_{tot}$ = 3.8 kcal mol^{-1}). The coordination sphere of the copper is distorted trigonal planar, with the bromine atom only slightly out of the plane formed by the phenanthroline backbone. The atoms Cu, Br, K, and O form an almost planar 4-membered ring. The K−Br (3.16 Å) and Cu−O (*ortho*: 2.77 Å) bonds are long, and the K−O (2.64 Å) and Cu−Br bonds (2.33 Å) are short. The forward motion along the reaction coordinate derived from the normal mode of the imaginary frequency (21 i cm^{-1}) is dominated by the shortening of the Cu−O distance. At the same time, the bromine atom moves out of the plane of the phenanthroline ligand.

In intermediate **20**, the copper atom is now in an almost tetrahedral environment. The K−Br (3.11 Å) and Cu−O (2.15 Å) bonds are further shortened and the K−O (2.66 Å) and Cu−Br bonds (2.41 Å) are elongated.

In the second phase of the anion exchange, a bromide leaves the copper center and eventually forms KBr. Stretching the Cu−Br bond leads to the transition state [**20**−**21**]‡. The activation barrier is rather low ($\Delta^{‡}E_{tot}$ = 5.2 kcal mol^{-1}, $\Delta^{‡}G_{sov}$ = 4.9 kcal mol^{-1}). The copper is in a distorted trigonal planar environment with the oxygen atom only slightly out of the plane of the phenanthroline backbone. The K−Br (3.04 Å) and Cu−O (1.91 Å) bonds are rather short, whereas the K−O (2.71 Å) and Cu−Br bonds are long (3.50 Å). The forward motion along the reaction coordinate derived from the normal mode of the imaginary frequency (21 i cm^{-1}) is dominated by the elongation of the Cu−Br bond and the motion of the oxygen atom into the plane of the phenanthroline ligand.

In the subsequent intermediate **21**, the Cu−Br bond is now fully broken while the K−Br (3.04 Å) and Cu−O (1.91 Å) bond lengths remain almost unchanged and the K−O bond is slightly elongated (2.74 Å).

For the *o*-fluoro model system, intermediate **21** finally dissociates into KBr (**10**) and the product of the anion exchange, the phenanthroline copper 2-fluorobenzoate (**1a**) that decarboxylates subsequently. Cleaving the K−O bond requires some energy (Δ_rE_{tot} = 25.3 kcal mol^{-1}), but the entropically favorable dissociation into two solvated molecules makes this step only slightly endergonic (Δ_rG_{sov} = 0.5 kcal mol^{-1}). The copper atom in **1a** is coordinated to only one of the carboxylate oxygens by a short bond (Cu−O: 1.89 Å) in a distorted trigonal planar environment. The nitrogen donor atoms of the phenanthroline ligand transfer sufficient electron density to the copper(I) cation so that this coordination mode is preferred, while for the electron-poor potassium cation, a coordination to both oxygen atoms is favorable (structure **7**).

The calculations further revealed that for 4-fluorobenzoate, the energy profile of the anion exchange is almost identical with that of the 2-fluorobenzoate (Figure 2, see also the Supporting Information). This result came as a surprise since decarboxylative cross-couplings of aryl halides with 2-fluorobenzoates are well-documented, while the analogous reactions of 4-fluorobenzoates have not yet been achieved. Only aryl electrophiles with noncoordinating groups such as triflates can be coupled with non-*ortho*-substituted benzoates. To rationalize these experimental findings, the salt metathesis of copper(I) halides with potassium benzoates had been postulated to be favorable for *ortho*-substituted derivatives, but unfavorable for non-*ortho*-substituted benzoates. This hypothesis was supported by protodecarboxylation experiments in which benzoic acids (**22**) were converted to the corresponding arenes (**23**) in the presence of a phenanthroline copper system according to Scheme 7. In the absence of halides, this reaction proceeded well both for *ortho*- and non-*ortho*-substituted benzoic acids. Upon the addition of a halide salt, the decarboxylation of non-*ortho*-substituted benzoic acids was fully suppressed, whereas the reactivity of the *ortho*-substituted benzoic acids remained high.[5]

Scheme 7. Influence of Halides on Protodecarboxylations

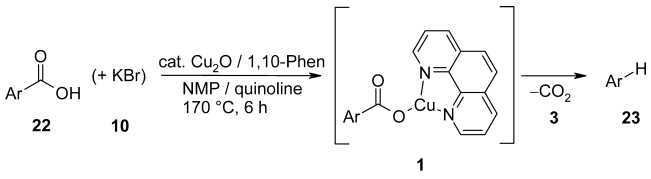

Ar = 2-F-C_6H_4: 91 % without KBr, 72 % with KBr
Ar = 4-F-C_6H_4: 27 % withoutKBr, 0 % with KBr

In a series of control experiments, similar observations were made also for the decarboxylation of the two fluorobenzoic acid isomers. The addition of 1 equiv of potassium bromide only slightly reduced the yield of the protodecarboxylation of 2-fluorobenzoic acid (**22a**) from 91% to 72% yield in the presence of potassium bromide. 4-Fluorobenzoic acid (**22b**) gave only 27% even in the absence of bromide ions, and when potassium bromide was added, the decarboxylation was completely suppressed.[46]

According to our present DFT studies, the salt exchange between the copper bromide species **11** and the fluorobenzoate isomers (**7a** and **7b**) is energetically very similar. It is slightly endergonic (*ortho*: Δ_rG_{sov} = 5.3 kcal mol^{-1}; *para*: Δ_rG_{sov} = 5.0

dx.doi.org/10.1021/ja503295x | J. Am. Chem. Soc. 2014, 136, 10007−10023

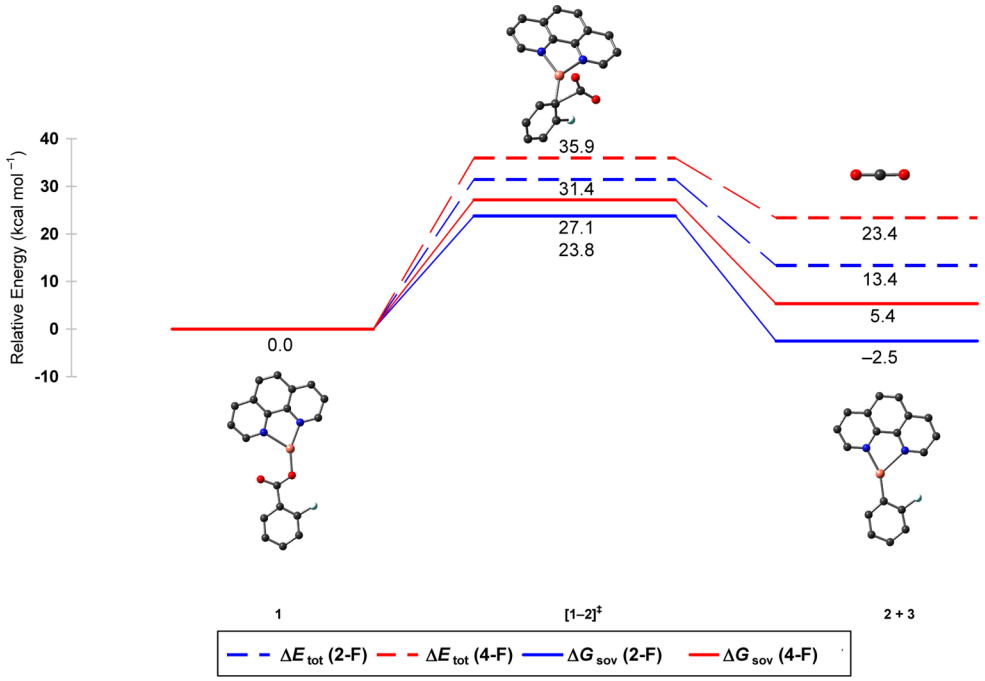

Figure 3. B3LYP/6-31+G(d) optimized structures for the decarboxylation of phenanthroline copper 2-fluorobenzoate; hydrogens are omitted for clarity. Energy and solution Gibbs energy profiles overlaid for 2- and 4-fluorobenzoate. Color code: C, black; Cu, orange; F, turquoise; N, blue; O, red.

kcal mol^{-1}) with low activation barriers. These calculations do not provide any rationale for the hypothesis that the presence of bromide ions suppresses the formation specifically of copper 4-fluorobenzoate complexes, so that the unique reactivity of *ortho*-substituted benzoates must have another reason. A precipitation of KBr, which would not be taken into account by the DFT calculations, is not observed in the experiment.

We therefore carefully explored alternative geometries for the salt exchange product phenanthroline copper 2-fluorobenzoate (**1a**), in which the carboxylate oxygen and the *o*-fluorine would both coordinate to the copper, potentially resulting in a more stable structure. This might be expected to lead to a substantially less endergonic anion exchange step for potassium 2-fluorobenzoate compared to 4-fluorobenzoate. However, no minima for complexes with chelating coordination were found.

We also investigated whether the energy profile is affected by leaving out the potassium counterion in the calculations. The resulting energy barriers are twice as high, and again, no differences of any potential consequence were found between 2- and 4-fluorobenzoates. The energy profiles along with the optimized structures can be found in Figure S1 in the Supporting Information.

Overall, the calculations do not support the previously postulated explanation for the effect of halide ions on the decarboxylation of non-*ortho*-substituted carboxylates. A possible explanation is that the additional bromide ions do not have an effect on the difference in reactivity of the *ortho*- and *para*-substituted benzoates in the anion exchange step but in the decarboxylation step that will be discussed in the next section. The presence of excess bromide salt shifts the equilibrium of the anion exchange step to the side of the copper bromide so that less copper carboxylate is available. This reduces the efficiency of the entire protodecarboxylation process. Since the decarboxylation of *ortho*-substituted benzoates requires less energy than that of non-*ortho*-substituted benzoates, high conversions of *ortho*-substituted benzoic acids can be achieved at temperatures where non-*ortho*-substituted derivatives do not decarboxylate.

Decarboxylation. The decarboxylation step has already been the subject of previous DFT investigations,[21c,22] because it was initially believed to be the only rate-determining step. We have now reinvestigated it using the high-quality basis set with diffuse functions detailed above, included solvent effects, dispersion interactions, and taken into account the concentrations and reaction temperatures.

The extrusion of carbon dioxide from phenanthroline copper 2-fluorobenzoate (**1**) was found to proceed via a concerted mechanism involving only one transition state ([**1**−**2**]‡, Figure 3). An extensive search did not reveal any further intermediates, such as π- or η^2-bound arene−copper complexes.

In the copper 2-fluorobenzoate **1a**, all atoms are coplanar. The two nitrogen−copper bond lengths of the phenanthroline ligand are slightly different (2.0 and 2.2 Å), which indicates that this ligand geometry is not ideal for Cu^{I}. The decarboxylation step can be viewed as a substitution of the carboxylate group by the copper center in a concerted fashion. The activation barrier for the extrusion of CO_2 from 2-fluorobenzoate is relatively high ($\Delta^{‡}E_{tot}$ = 31.4 kcal mol^{-1}, $\Delta^{‡}G_{sov}$ = 23.8 kcal mol^{-1}), but within a realistic range for a reaction that requires a temperature of 160 °C. In the transition state [**1a**−**2a**]‡, the copper atom is in a distorted tetrahedral environment formed by the two phenanthroline nitrogens, the 2-fluorophenyl and the CO_2 carbons. The Cu−N bonds have similar lengths (ca. 2.1 Å). The fluorophenyl moiety binds to both the copper and the CO_2 carbon via its C(1) carbon. The aryl−CO_2 bond is short (1.94 Å) while the aryl−copper bond is relatively long (2.02 Å), which is indicative for a relatively early transition state. The forward motion along the reaction coordinate derived from the normal mode of the imaginary frequency (229

dx.doi.org/10.1021/ja503295x | J. Am. Chem. Soc. 2014, 136, 10007−10023

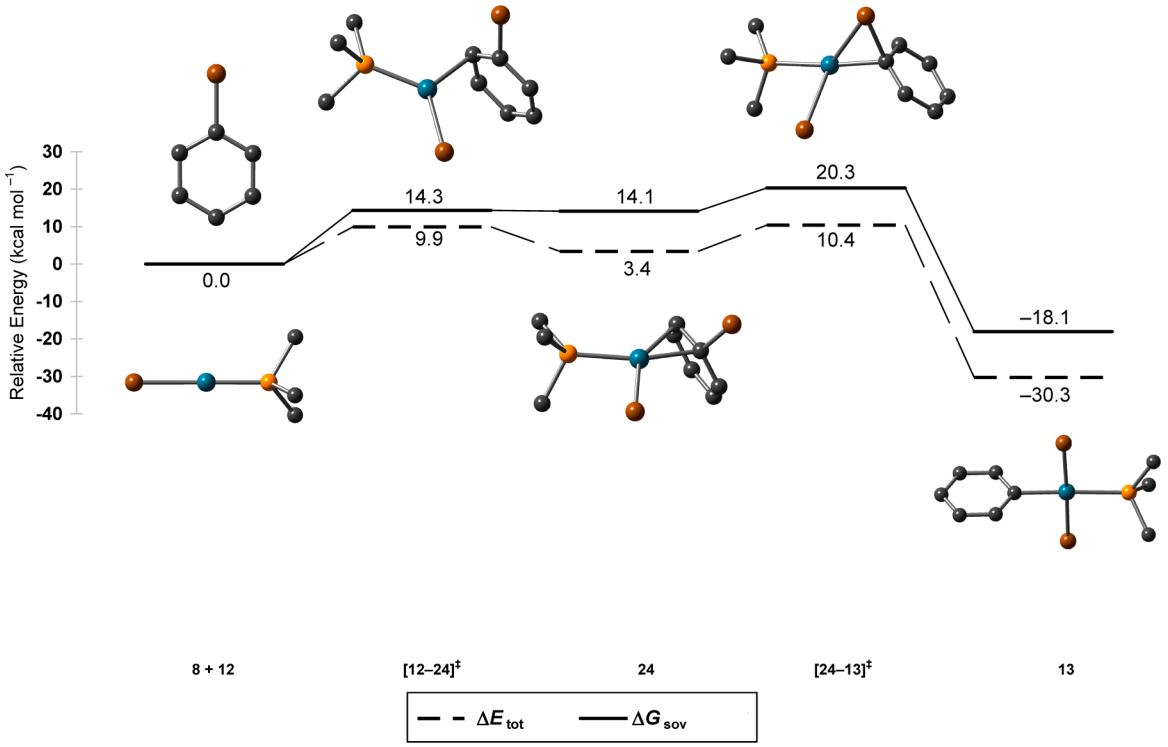

Figure 4. B3LYP/6-31+G(d) optimized structures for the oxidative addition of bromobenzene to $[Pd(PMe_3)Br]^-$; hydrogens are omitted for clarity. Color code: C, black; Br, brown; P, yellow; Pd, green.

i cm^{-1}) is dominated by the elongation of the aryl−CO_2 bond with a concomitant contraction of the aryl−copper bond.

The IRC calculation reveals that the transition state directly leads to the decarboxylation product **2a**. The 2-fluorophenyl ring remains in the plane of the phenanthroline backbone. A weak interaction between a fluorine lone pair and the hydrogen at C(2) of the phenanthroline scaffold, which are separated by a distance of only 2.30 Å, additionally stabilizes this geometry. The phenanthroline coordination is even more asymmetrical than prior to decarboxylation, with Cu−N bonds of 2.0 and 2.4 Å, respectively.

Overall, the decarboxylation of 2-fluorobenzoate is moderately endothermic (Δ_rE_{tot} = 13.4 kcal mol^{-1}). Whereas in the previous, simplified calculations, the decarboxylation had come out endergonic, the present, more refined calculations predict it to be exergonic (Δ_rG_{sov} = −2.5 kcal mol^{-1}) at the calculated reaction temperature of T = 443.15 K. Among other effects, the entropy gained by releasing CO_2 contributes more strongly to the Gibbs energy because we take into account the higher reaction temperature.

The pathway for the decarboxylation of 4-fluorobenzoate is slightly different. The activation barrier for the extrusion of CO_2 is considerably higher ($\Delta^‡E_{tot}$ = 35.9 kcal mol^{-1}, $\Delta^‡G_{sov}$ = 27.1 kcal mol^{-1}), which is in good agreement with the experimental findings that the protodecarboxylation of non-*ortho*-substituted benzoic acids requires higher temperatures and longer reaction times than that of *ortho*-substituted derivatives.[21c] In contrast to the decarboxylation of 2-fluorobenzoate, the transition state originating from 4-fluorobenzoate [**1b**−**2b**]‡ has a long aryl−CO_2 bond (2.06 Å) and a short aryl−copper bond (1.98 Å). This is indicative of a later transition state, which suggests that the decarboxylation is more endergonic for this isomer. The formation of **2b** is indeed strongly endothermic (Δ_rE_{tot} = 23.4 kcal mol^{-1}), but due to the entropically favorable liberation of CO_2, it is only slightly endergonic (Δ_rG_{sov} = 5.4 kcal mol^{-1}). The structure of the decarboxylation product **2b** differs from that for the *ortho*-derivative **2a** in that the 4-fluorophenyl ring is rotated out of the plane of the phenanthroline backbone at an angle of 55.7°, which may be caused by the absence of a hydrogen−fluorine interaction. Overall, the decarboxylation of non-*ortho*-substituted benzoates is both kinetically and thermodynamically significantly less favorable than the analogous reaction of *ortho*-substituted benzoates, a result that is in perfect agreement with experimental observations of protodecarboxylations.[21c]

Oxidative Addition. The catalytic cycle of palladium starts with the oxidative addition of the aryl halide to a Pd^0 species. When starting from the anionic palladium monophosphine complex $[Pd(PMe_3)Br]^-$ (**12**), this reaction step proceeds with particular ease (Figure 4). Upon bringing the bromobenzene (**8**) closer to the palladium center, an η^2-π-complex (**24**) forms via the transition state [**12**−**24**]‡. The activation barrier for this step is rather low for a process in which a bond forms between two separately solubilized molecules ($\Delta^‡E_{tot}$ = 9.9 kcal mol^{-1}, $\Delta^‡G_{sov}$ = 14.3 kcal mol^{-1}). This difference stems from entropy and solvation as discussed above. In the transition state, a bond between the palladium and the C(2) atom of bromobenzene has already formed (Pd−C(2): 2.31 Å), and the previously linear Br−Pd−P bond is bent at an angle of 125.4°. The forward motion along the reaction coordinate derived from the normal mode of the imaginary frequency (62 i cm^{-1}) is dominated by the shortening of the Pd−C(1) and Pd−C(2) distances with simultaneous decrease of the Br−Pd−P angle.

The IRC calculation leads to intermediate **24**, in which the palladium atom is coordinated almost symmetrically to the π-bond between C(1) and C(2) (Pd−C(1): 2.11 Å; Pd−C(2): 2.18 Å). The C−Br bond is slightly elongated from 1.92 to 2.00 Å, and the Br−Pd−P angle has decreased to 90.8°.

dx.doi.org/10.1021/ja503295x | J. Am. Chem. Soc. 2014, 136, 10007−10023

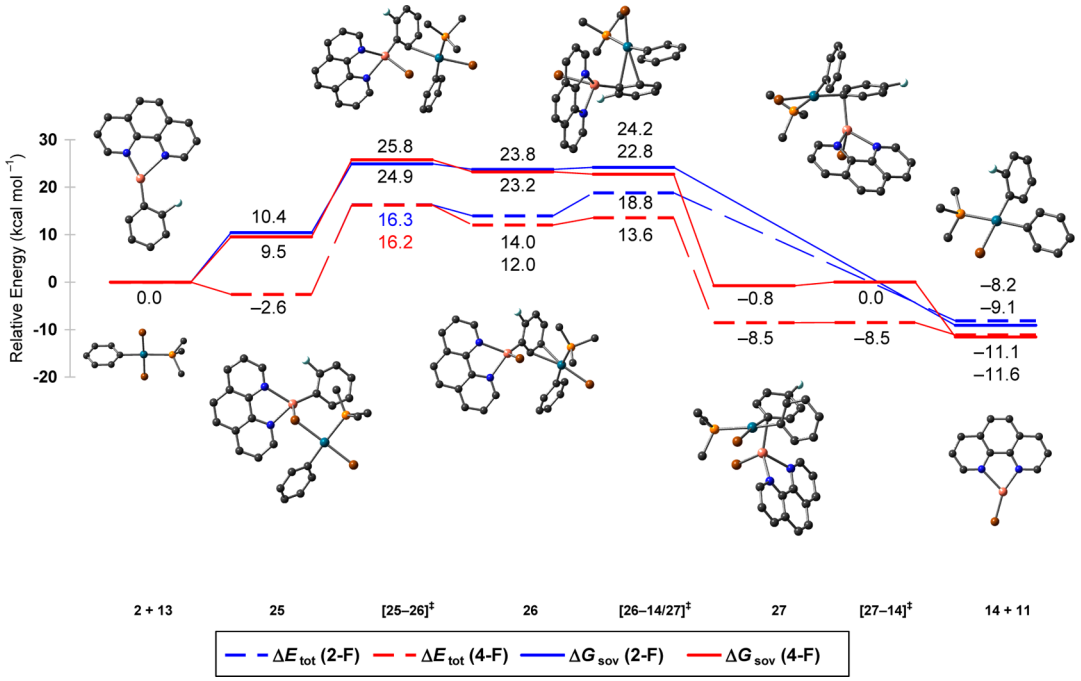

Figure 5. B3LYP/6-31+G(d) optimized structures for the transmetalation of the phenanthroline copper 2-fluorophenyl complex (**2**) with $[Pd(PMe_3)(Ph)Br_2]^-$ (**13**); hydrogens are omitted for clarity. Energy and solution Gibbs energy profiles overlaid for the 2- and 4-fluorophenyl derivative. Color code: C, black; Br, brown; Cu, orange; F, turquoise; N, blue; P, yellow; Pd, green.

Further shortening of the Pd−C(1) bond leads to another transition state [**24**−**13**]‡, that has a Pd−C(1) bond length of 2.03 Å, and in which a Pd−Br bond is starting to form (2.89 Å). The C−Br bond is elongated to 2.22 Å. The forward motion along the reaction coordinate derived from the normal mode of the imaginary frequency (126 i cm^{-1}) is dominated by the movement of the palladium atom into the plane of the aromatic ring, resulting in a shortening of the Pd−C(1) bond, while the bromine moves out of this plane with concomitant elongation of the C−Br bond. The activation barrier for this step is rather low ($\Delta^{‡}E_{tot}$ = 7.0 kcal mol^{-1}, $\Delta^{‡}G_{sov}$ = 6.2 kcal mol^{-1}).

In the final oxidative addition product, the trimethylphosphino(phenyl)dibromopalladate **13**, the palladium is in a slightly distorted square-planar environment with the two bromine ligands *trans* to each other. The Pd−Br(1) and Pd−Br(2) bonds have almost the same lengths (2.54 and 2.52 Å), and the Pd−C distance amounts to 2.03 Å.

The overall oxidative addition process is strongly exothermic (Δ_rE_{tot} = −30.3 kcal mol^{-1}), and although two molecules are converted to one product, it remains exergonic (Δ_rG_{sov} = −18.1 kcal mol^{-1}). Under the reaction conditions of the decarboxylative coupling, the oxidative addition can be expected to proceed very smoothly.

Transmetalation. In the transmetalation step, the phenanthroline copper 2- or 4-fluorophenyl complex **2**, obtained by decarboxylation of copper 2- or 4-fluorophenyl benzoate, has to approach the palladium complex **13**, formed by the oxidative addition, in order to transfer the fluorophenyl group to the palladium center. One would expect to find that the actual transmetalation step would be preceded by the formation of an energetically favorable adduct between **2** and **13**, which would explain that this entropically unfavorable step takes place even at the low experimental concentrations of the two species.

We first sought for attractive interactions between **2a** and **13** by positioning the two fragments close to each other at various angles and orientations. Whereas no energetically favorable interaction was found, e.g., when approaching the palladium and the π-system of the fluorophenyl ring, bringing palladium complex **13** into close proximity to the copper atom in **2a** via its bromine ligand results in the formation of a stable adduct (**25a**, Figure 5). The formation of a long Cu−Br(1) bond (2.82 Å) makes this step energetically favorable (Δ_rE_{tot} = −2.6 kcal mol^{-1}), which makes up for some of the high entropic hurdle and loss of solvation energy associated with forming an adduct at high reaction temperatures. In the present case, the amount of entropy lost is 33.4 cal K^{-1} mol^{-1}, which at 443 K increases Δ_rG_{sov} by 14.8 kcal mol^{-1}. The dispersion interaction additionally stabilizes the adduct by 13.1 kcal mol^{-1}, whereas 9.1 kcal mol^{-1} solvation energy is lost. Together, these factors turn a slightly exothermic step into a moderately endergonic one (Δ_rG_{sov} = 10.4 kcal mol^{-1}). The additional Cu−Br(1) bond changes the coordination environment at the copper center from a coordinatively unsaturated distorted trigonal planar arrangement to a distorted tetrahedral geometry (∠Cu−Br−Pd = 108.8°). The formation of the loose Cu−Br(1) contact (2.82 Å) does not lead to a significant elongation of the Pd−Br(1) bond (2.53 Å), and the geometry of the palladium fragment remains almost unchanged. The fluorophenyl group is bent outward slightly, but is not twisted. A transit scan from **25** with a stepwise elongation of the Cu−Br(1) bond revealed that in the gas phase, the encounter complex **25** is formed without a barrier.

Adduct **25** was found to be the entry point to a transmetalation pathway in which the bromine ligand is transferred from palladium to copper prior to transfer of the fluorophenyl group in the opposite direction. A search for alternative transmetalation pathways in which, for example, the transfer of the fluorophenyl group from Cu to Pd precedes that of the bromine ligand from Pd to Cu, did not yield any results.

dx.doi.org/10.1021/ja503295x | J. Am. Chem. Soc. 2014, 136, 10007−10023

This was to be expected in the absence of attractive interactions between the fluorophenyl group and the copper.

Shortening the Cu−Br(1) bond of **25a** to 2.54 Å leads to an energetically reasonable transition state [**25a**−**26a**]‡ ($\Delta^{‡}E_{tot}$ = 18.9 kcal mol^{-1}, $\Delta^{‡}G_{sov}$ = 14.5 kcal mol^{-1}). In [**25a**−**26a**]‡, the palladium is coordinated to the C(2) carbon of the fluorophenyl group over a rather long bond (2.59 Å), while the Pd−Br(1) bond is almost broken (3.65 Å). The tetrahedral environment at the copper is now more symmetrical than in adduct **25a**. The forward motion along the reaction coordinate derived from the normal mode of the imaginary frequency (30 i cm^{-1}) is dominated by the elongation of the Pd−Br(1) bond with a simultaneous shortening of the Pd−C(2) and Pd−C(3) distances. The IRC calculation confirms that this transition state leads to intermediate **26a**, in which the palladium atom is coordinated to the C(2)−C(3) π-bond in an almost symmetrical fashion (Pd−C(2): 2.48 Å; Pd−C(3): 2.52 Å). The Cu−Br(1) bond is slightly shortened to 2.51 Å. Intermediate **26a** is almost as high in energy as the transition state.

Starting from **25a**, no trajectory could be found along which the palladium would directly attack the C(1) carbon of the fluorophenyl group, so that the transfer of the bromine and of the fluorophenyl group would occur in a single step. This finding corresponds well with those for several oxidative addition and transmetalation pathways of other aromatic substrates, which also have been found to involve the intermediate formation of π-complexes to the C(2)−C(3) bond of the arene rings.[24b,47]

Shortening the Pd−C(1) distance leads to a transition state [**26a**−**14a**]‡ across a rather low activation barrier ($\Delta^{‡}E_{tot}$ = 4.8 kcal mol^{-1}, $\Delta^{‡}G_{sov}$ = 0.4 kcal mol^{-1}). In [**26a**−**14a**]‡, the palladium atom has shifted to the C(1)−C(2) π-bond of the fluorophenyl group. The Pd−C(1) bond is slightly longer than the Pd−C(2) bond (Pd−C(1): 2.82 Å; Pd−C(2): 2.60 Å). The copper atom remains in the plane of the fluorophenyl ring, and the Cu−C(1) bond has the same length as in **26a** (1.96 Å). The distance between the copper and palladium atoms is reduced to only 3.30 Å. The forward motion along the reaction coordinate derived from the normal mode of the imaginary frequency (59 i cm^{-1}) is dominated by a lengthening of the Pd−C(2) bond with concomitant shortening of the Pd−C(1) and Cu−Pd bonds, resulting in the transfer of the fluorophenyl group from copper to palladium.

At first sight, it seemed counterintuitive that the copper atom would remain in the plane of the arene ring in transition state [**26a**−**14a**]‡, and that the Cu−C(1) bond length would not significantly contribute to the normal mode corresponding to the imaginary frequency. We would have expected a transition state structure in which the copper would already have moved out of the plane of the fluorophenyl ring and the Cu−C(1) bond would already have been elongated. We therefore investigated the pathway from [**26a**−**14a**]‡ to the transmetalation products **14a** + **11** in some detail by IRC calculations, followed by geometry optimizations. On the way downhill, we came across regions of the potential energy surface with molecular geometries meeting our above expectations, but found no stationary points. Instead, this process confirmed that the transition state [**26a**−**14a**]‡ indeed connects intermediate **26a** with the transmetalation products **14a** + **11**. The somewhat surprising structural features of the transition state are a consequence of its being very early, which conforms to the Hammond postulate.[48] Aryl transfer and separation into two fragments occur simultaneously in this final phase of the transmetalation, which is therefore quite exothermic ($\Delta_r E_{tot}$ = −22.2 kcal mol^{-1}) and even more exergonic ($\Delta_r G_{sov}$ = −32.9 kcal mol^{-1}), because of the substantial gain in entropy and solvation energy.

The products of the transmetalation are the regenerated phenanthroline copper bromide catalyst **11**, which was already described in the anion exchange chapter, and the square-planar *cis*-diaryl palladium complex **14a**. Its Pd−C(1) bond length is further shortened to 2.04 Å, which is almost the same as that of the Pd−C(1′) bond of 2.05 Å. Overall, the entire transmetalation starting from **2a** and **13** and leading to **11** and **14a** is moderately exothermic ($\Delta_r E_{tot}$ = −8.2 kcal mol^{-1}) and exergonic ($\Delta_r G_{sov}$ = −9.1 kcal mol^{-1}).

The reaction pathway for the transfer of the 4-fluorophenyl group from the aryl copper complex **2b** to the palladium complex **13** is different from that of the 2-fluorophenyl complex **2a**. Both the geometries and the energies of several structures involved are markedly different. Moreover, an additional intermediate is involved in the transmetalation for the 4-fluorophenyl derivative.

Adduct **25b** and the first transition state [**25b**−**26b**]‡ have closely related structural features and relative energies to their *ortho*-regioisomers. Compared to **26a**, intermediate **26b** is lower in energy by −2.0 kcal mol^{-1} and the Gibbs energy is lower by −0.6 kcal mol^{-1}. According to our calculations, this can be attributed to the energy of solvation and explained with greater structural differences between these intermediates. After elongation of the Pd−Br contact in [**25**−**26**]‡, the 4-fluorophenyl group rotates around the Cu−C bond, which does not occur with the 2-fluorophenyl group. The structures of **26a** and **26b** provided in the Supporting Information are displayed with the fluorophenyl groups and coordinated palladium fragments in the same orientation. In **26a**, the phenanthroline points to the left and the bromine to the right of the copper. In **26b**, the phenanthroline points downward and the bromine upward. The Cu−Br bond in **26b** is somewhat longer (2.60 Å) than in [**25b**−**26b**]‡ (2.52 Å). The Pd−C(2) bond in **26b** is shorter by ca. 0.2 Å compared to the Pd−C(3) bond (Pd−C(2): 2.41 Å; Pd−C(3): 2.60 Å).

The energetic hurdle between **26b** and the transition state [**26b**−**27**]‡ amounts to $\Delta^{‡}E_{tot}$ = 1.6 kcal mol^{-1}. This barrier is only one-third as high as that for the *ortho*-substituted derivative and can again be attributed to structural differences. The Pd−C(2) bond is slightly shorter (2.46 Å) than in [**26a**−**14a**]‡ (2.60 Å), and the distance between copper and palladium of 3.55 Å in [**26b**−**27**]‡ is longer compared to 3.30 Å in [**26a**−**14a**]‡.

In contrast to the *ortho*-intermediate, **26b** does not lead to the transmetalation products **14b** + **11** in a single step. It involves an additional intermediate **27** in which the palladium fragment is in a nearly square-planar environment. The palladium atom has almost moved into the plane of the fluorophenyl ring, and the Pd−C(1) bond has shortened to 2.10 Å. The copper atom has moved below the plane of the fluorophenyl ring but is still connected to its *ipso* carbon over a very long Cu−C(1) bond (2.32 Å). The Pd−C(1)−Cu angle of 77.8° is very small, so that the two transition metals are in close proximity to each other. The Pd−Cu distance is as short as 2.77 Å, which is smaller than the sum of their van der Waals radii (3.03 Å).[49] Completing the transmetalation from intermediate **27** requires only little activation energy (transition state [**27**−**14b**]‡: $\Delta^{‡}E_{tot}$ = 0.0 kcal mol^{-1}, $\Delta^{‡}G_{sov}$ = 0.8 kcal mol^{-1}), so that the existence or nonexistence of the intermediate virtually has

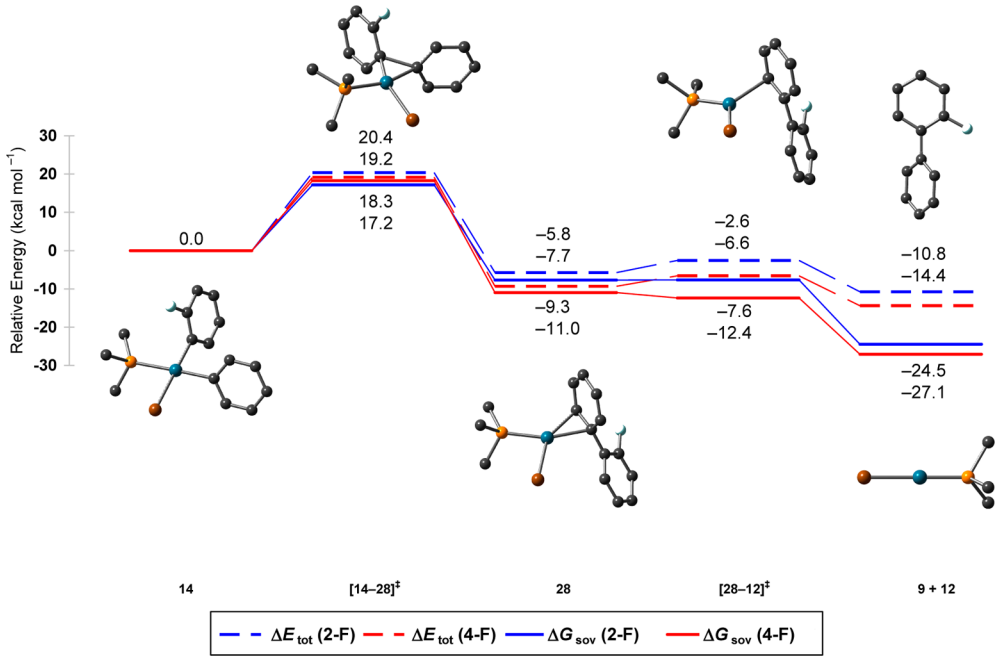

Figure 6. B3LYP/6-31+G(d) optimized structures for the reductive elimination of $[Pd(PMe_3)(2\text{-}F\text{-}Ph)(Ph)Br]^-$; hydrogens are omitted for clarity. Energy and solution Gibbs energy profiles overlaid for the 2- and 4-fluorophenyl derivative. Color code: C, black; Br, brown; F, turquoise; P, yellow; Pd, green.

no effect on the reactivity. Still, we invested some effort in finding a corresponding intermediate for the *ortho*-case. Thus, the optimized structure **27** was transformed into its *ortho*-derivative by replacing F by H and either of the two *o*-hydrogens by fluorine. However, for either of these structures, new geometry optimizations directly led to the transmetalation products. The existence of the intermediate **27** for the *para*- but not the *ortho*-case may be explained with electronic effects due to the fluorine substituent. The mesomeric effects of the fluorine substituent are comparable for the *ortho*- and *para*-positions, but the inductive effect on the *ipso* carbon of the fluorine in the *ortho*-position is certainly higher due to the smaller number of interjacent σ-bonds. In the 4-fluorophenyl ring, the electron-donating mesomeric effect of the fluorine predominates over the inductive effect and pushes sufficient electron density into the *ipso*-carbon to bind both transition metals simultaneously and lending stability to intermediate **27**. Contrarily, in the 2-fluorophenyl ring, the short-range electron-withdrawing inductive effect outweighs the mesomeric effect. The *ipso*-carbon thus lacks the electron density required to coordinate to palladium and copper at the same time.

Intermediate **27** features the shortest Pd−Cu distance (2.77 Å) observed in all these calculations. This begs the question whether there is an interaction or even a bond between copper and palladium. This is very difficult to answer with DFT calculations. Methods such as the analysis of the natural bond order (NBO), the bond critical point (BCP), or the shared electron number (SEN) with DFT are often regarded as inconclusive. Therefore, we looked for literature on bimetallic complexes with similarly short copper−palladium distances in which metal−metal interactions and bonds are discussed.

Kawamura et al. crystallized $[Pd_3(S_2CN^nPr_2)_6Cu_2][PF_6]_2$ and found slightly longer Pd−Cu distances of 2.864(4) and 2.896(4) Å.[50] Their XPS binding studies suggest weak Pd−Cu bonding interactions. However, the authors were unable to prove the existence of direct Pd−Cu bonding. Peng and Rohmer crystallized $[Cu_2Pd(dpa)_4Cl_2]$ (dpa = dipyridylamine) with somewhat shorter Pd−Cu distances of 2.4971(3) and 2.5022(3) Å.[51] For this complex, magnetic susceptibility measurements revealed an antiferromagnetic coupling between the two Cu^{II} metal centers connected to the Pd atom, which could be confirmed by powder EPR experiments, DFT calculations, and wave function theory calculations.[52] Osakada et al. observed Pd−Cu distances of 2.462(1) and 2.632(1) Å in crystallized $[Pd(\mu\text{-}CuI)(Pd(dmpe))_3(\mu_3\text{-}GePh_2)_3]$.[53] ^1H and $^{13}C\{^1H\}$ NMR experiments of the complex at various temperatures revealed that Cu forms a stable Pd−Cu bond to the core palladium and a labile Pd−Cu bond to one edge palladium. Because interactions or even bonds between copper and palladium could be proven for these complexes, which all possess short Pd−Cu distances in the same range as our intermediate **27**, we believe that attractive interactions between the copper and palladium atoms are at play also in the transmetalation step of decarboxylative cross-couplings.

Overall, our DFT results show that the transmetalation process is exothermic (*ortho*: $\Delta_rE_{tot} = -8.2$ kcal mol^{-1}; *para*: $\Delta_rE_{tot} = -11.1$ kcal mol^{-1}) as well as exergonic (*ortho*: $\Delta_rG_{sov} = -9.1$ kcal mol^{-1}; *para*: $\Delta_rG_{sov} = -11.6$ kcal mol^{-1}). However, the process starts with the formation of a bimetallic adduct that is endergonic (*ortho*: $\Delta_rG_{sov} = 10.4$ kcal mol^{-1}; *para*: $\Delta_rG_{sov} = 9.5$ kcal mol^{-1}). Furthermore, the transmetalation faces high activation barriers for its transition states that we will compare with those for the other elementary steps at the end of this section.

Reductive Elimination. In the reductive elimination step, the biaryl product **9** is liberated from the square-planar *cis*-diarylpalladium complex **14**, regenerating the initial palladium catalyst **12** (Figure 6). Both for the *ortho*- and the *para*-substituted model compounds, the overall process is moderately exothermic (*ortho*: $\Delta_rE_{tot} = -10.8$ kcal mol^{-1}; *para*: $\Delta_rE_{tot} = -14.4$ kcal mol^{-1}) and strongly exergonic (*ortho*: $\Delta_rG_{sov} =$

dx.doi.org/10.1021/ja503295x | J. Am. Chem. Soc. 2014, 136, 10007−10023

Scheme 8. Anionic Reaction Pathways Investigated for the Anion Exchange, Decarboxylation, and Adduct Formation

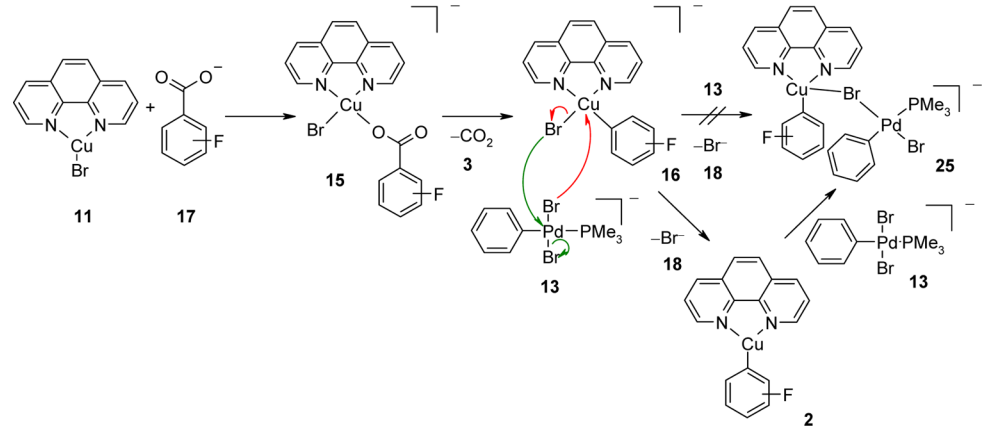

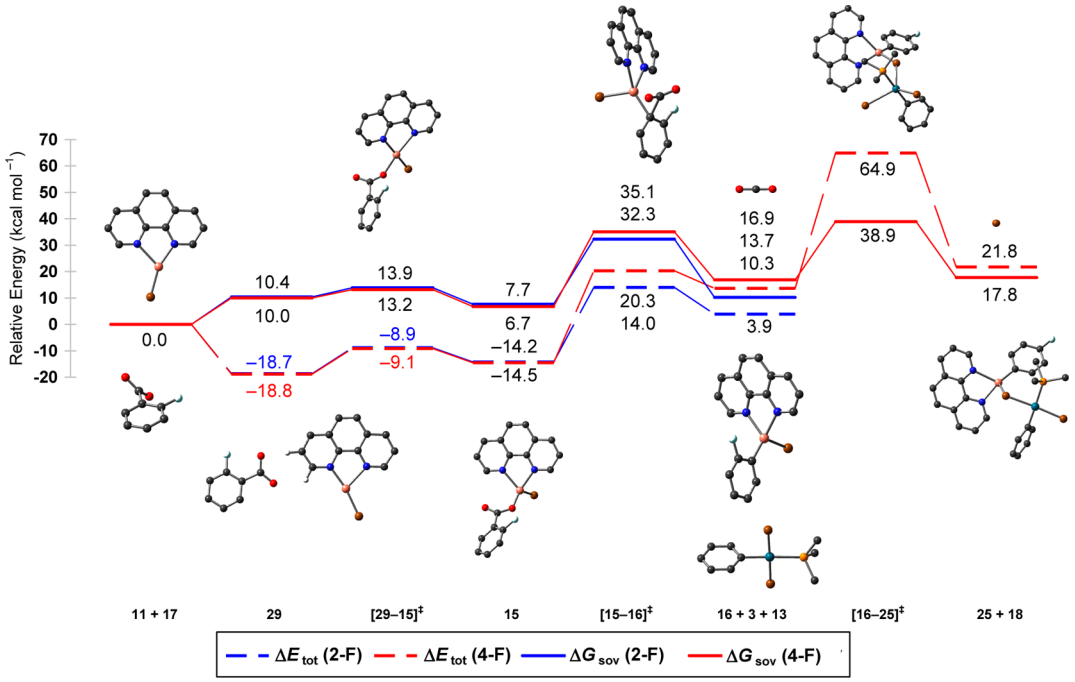

Figure 7. B3LYP/6-31+G(d) optimized structures for the anionic reaction pathway for anion exchange, decarboxylation, and adduct formation; hydrogens are omitted for clarity. Energy and solution Gibbs energy profiles overlaid for 2- and 4-fluorobenzoate. Color code: C, black; Br, brown; Cu, orange; F, turquoise; N, blue; O, red; P, yellow; Pd, green.

−24.5 kcal mol^{-1}; *para*: $\Delta_r G_{sov}$ = −27.1 kcal mol^{-1}), since two molecules form from one.

Starting from **14a**, a first transition state [**14a**−**28a**]‡ was found by reducing the C(1) and C(1′) distance between the two aromatic rings in the square-planar complex to 1.88 Å. The barrier for its formation is comparatively low ($\Delta^{‡}E_{tot}$ = 20.4 kcal mol^{-1}, $\Delta^{‡}G_{sov}$ = 17.2 kcal mol^{-1}). The Pd−C bond lengths and the P−Pd−Br angle remain almost unchanged (Pd−C(1): 2.07 Å; Pd−C(1′): 2.11 Å; P−Pd−Br: 88.6°). The forward motion along the reaction coordinate derived from the normal mode of the imaginary frequency (306 i cm^{-1}) is dominated by a shortening of the aryl−aryl bond, while the angle between the planes of the aromatic rings is reduced.

An IRC calculation revealed that transition state [**14a**−**28a**]‡ connects structure **14a** with intermediate **28a**. In **28a**, the aryl−aryl bond is fully formed with a final length of 1.49 Å, but the palladium remains η^2-coordinated to the C(1′)−C(2′) bond of the biaryl product (Pd−C(1′): 2.25 Å; Pd−C(2′): 2.17 Å; P−Pd−Br: 94.7°).

The energy barrier for the release of the Pd(0) catalyst **12** is very low ($\Delta^{‡}E_{tot}$ = 3.2 kcal mol^{-1}, $\Delta^{‡}G_{sov}$ = 0.03 kcal mol^{-1}). In the transition state [**28a**−**12a**]‡, which was found by increasing the distance between palladium and the phenyl ring, the palladium atom remains coordinated to C(2′) over a distance of 2.35 Å, and the P−Pd−Br angle has increased to 126.1°. The forward motion along the reaction coordinate derived from the normal mode of the imaginary frequency (54 i cm^{-1}) is dominated by a lengthening of the Pd−C bond with simultaneous opening of the P−Pd−Br angle (Pd−C(2′): 2.35 Å; P−Pd−Br: 126.1).

A further IRC calculation showed that this transition state connects directly to the linear anionic monophosphine palladium complex **12** and the biaryl **9a**. In **9a**, the angle between the planes of the two aromatic rings amounts to 44.3°.

dx.doi.org/10.1021/ja503295x | J. Am. Chem. Soc. 2014, 136, 10007−10023

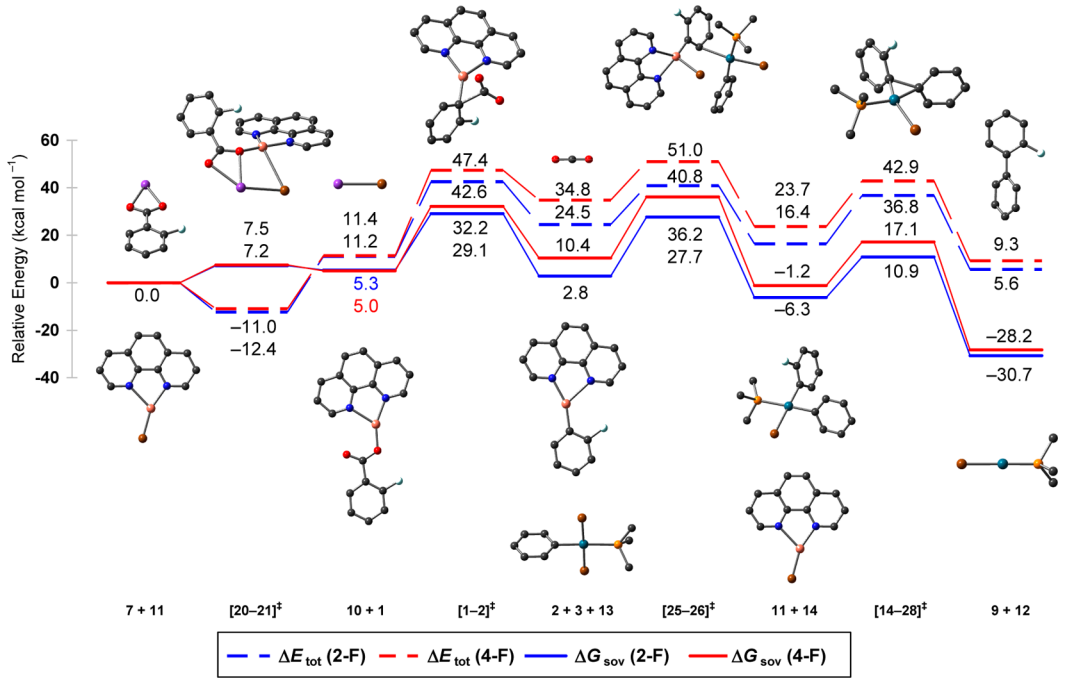

Figure 8. B3LYP/6-31+G(d) optimized structures for the simplified reaction profile; hydrogens are omitted for clarity. Energy and solution Gibbs energy profiles overlaid for the 2- and 4-fluorophenyl derivative. Color code: C, black; Br, brown; Cu, orange; F, turquoise; K, purple; N, blue; O, red; P: yellow; Pd, green.

As can be seen in Figure 6, the reaction pathway for the 4-fluorophenyl derivative is almost identical with that for the 2-derivative. The main activation barrier ($\Delta^{\ddagger}E_{tot}$ = 19.2 kcal mol^{-1}, $\Delta^{\ddagger}G_{sov}$ = 18.3 kcal mol^{-1}) and the imaginary frequency of the transition state [**14b**−**28b**]‡ (316 i cm^{-1}) are almost identical with those for the 2-derivative. In biaryl **9b**, the dihedral angle is slightly smaller than in **9a** (41.4° versus 44.3°), since the *o*-hydrogen requires less space than the fluorine atom.

Anionic Copper Cycle. In the transformations discussed above, all Cu^{I} intermediates were neutral and tricoordinated. An alternative pathway can be envisaged in which the carboxylate anion adds to copper complex **11** leading to a tetracoordinate anionic copper species, which after extrusion of CO_2 undergoes the transmetalation (Scheme 8). In this alternative pathway, the equivalent to the anion exchange step would be the coordination of the carboxylate **17** to the copper complex **11**. The resulting anionic copper complex **15** would decarboxylate to the anionic copper complex **16**. Complex **16** would then react with the palladium catalyst **13** in an associative substitution reaction to give adduct **25**, which would be the starting point for the transmetalation process. Alternatively to this associative pathway, one could also imagine that the bromide would decoordinate from **16** to give the fluorophenyl copper phenanthroline complex **2**, which would associate with **13** to give the adduct **25**. The energy and solution Gibbs energy profiles for the anionic pathway (**11** → **15** → **16** → **25**) are shown in Figure 7.

The formation of adduct **15a** from 2-fluorobenzoate **17a** and the copper complex **11** is exothermic ($\Delta_r E_{tot}$ = −14.2 kcal mol^{-1}) in the gas phase and proceeds via an encounter complex **29a** and a transition state [**29a**−**15a**]‡. Due to the loss of entropy and solvation energy, this step is endergonic ($\Delta_r G_{sov}$ = 7.7 kcal mol^{-1}), with a barrier ($\Delta^{\ddagger}G_{sov}$ = 13.9 kcal mol^{-1}) that is higher than in the neutral anion exchange pathway (see Figure 2).

The anionic copper complex **15a** can then directly decarboxylate via transition state [**15a**−**16a**]‡, instead of first releasing the bromine ligand. The Gibbs activation energy of $\Delta^{\ddagger}G_{sov}$ = 24.6 kcal mol^{-1} is higher than that for the decarboxylation of the neutral phenanthroline copper 2-fluorobenzoate **1a** ($\Delta^{\ddagger}G_{sov}$ = 23.8 kcal mol^{-1}).

Two pathways are imaginable for the associative substitution reaction of the anionic copper complex **16** with the palladium catalyst **13** each leading to formation of a bromine bridge between the two metals. One of the Pd-bound bromide ligands may attack the copper center and replace its bromide (red arrows, Scheme 8), or conversely the Cu-bound bromide may attack the palladium center with loss of a Pd-bound bromide (green arrows). For the first pathway, we were unable to find any feasible pathway in our DFT calculations. For the second, a transition state [**16b**−**25b**]‡ could be located only for the *p*-fluoro-substituted derivative. The activation barrier is very high ($\Delta^{\ddagger}E_{tot}$ = 51.2 kcal mol^{-1}, $\Delta^{\ddagger}G_{sov}$ = 22.0 kcal mol^{-1}). For the *ortho*-derivative **16a**, the only pathway we found required dissociation of the bromide. This dissociation of bromide is thermodynamically downhill for both the *ortho*- and the *para*-derivative (**16a**/**16b**), and leads to the phenanthroline copper fluorophenyl complex **2a**/**2b**, so that the neutral pathway is re-entered. When similar calculations were performed with potassium ions, we found direct elimination of KBr and a direct re-entry into the neutral pathway. Overall, the anionic complexes **15a**/**b** do not open up a pathway with a low energy profile that is more favorable for *ortho*- than for non-*ortho*-substituted benzoates and could explain why the former substrates react more readily in decarboxylative couplings.

Summary Assessment of the Catalytic Cycle. Improving a catalyst based on theoretical modeling requires a recipe for extracting the catalyst efficiency from the plethora of energetic data obtained in the calculations. The energetic span concept by Amatore and Jutand[54] says that the largest possible

dx.doi.org/10.1021/ja503295x | J. Am. Chem. Soc. 2014, 136, 10007−10023

rate and, correspondingly, the highest turnover number of the catalytic cycle is obtained for the lowest Gibbs energy span, which is the Gibbs energy difference between the highest transition state and lowest intermediate of the entire cycle. This concept has been refined by Kozuch and Shaik[55] by taking into account overall exergonicity. In our case, the situation is more complicated because of the two intertwined catalytic cycles, which join and separate at the transmetalation. The approximation behind the energy span concept is that the concentration c_i of a catalyst intermediate i is given by $c_i = c_0 \exp(-\Delta G_i/RT)$, where c_0 is the overall catalyst concentration and ΔG_i the Gibbs energy of i with respect to the most stable intermediate, where most of the catalyst is trapped. Both our calculated energy profile and our experience with related catalytic reactions tell us that the palladium catalyst is capable of providing the oxidative addition product **13** at a much faster rate than the cross-coupling proceeds, and according to our calculations, the oxidative addition is exergonic ($\Delta_r G = -18.1$ kcal mol^{-1}). Therefore, we can simplify the kinetic model by assuming that the stationary concentration of **13** is given by the overall amount of palladium catalyst. In other words, we consider a reaction with a single catalytic cycle in which one of the educts is **13** at its catalytic concentration, instead of the aryl bromide **8** at a stoichiometric concentration. We then apply the energetic span concept to the energy profile derived from this single cycle, which involves four steps (anion exchange, CO_2 extrusion, transmetalation, reductive elimination). Since none of these steps feature an intermediate lower in Gibbs energy than either their educts or their products, we need only consider a single effective activation energy given by the highest transition state of each step. This resulting simplified energy diagram is shown in Figure 8.

The energy barriers of this simplified reaction profile with the highest barrier at $\Delta^{\ddagger}G_{sov} = 36.2$ kcal mol^{-1} are consistent with a reaction that takes place at temperatures around 160 °C.

For the *ortho*-case, the largest Gibbs energy span, which represents the apparent activation energy of the overall cycle, is between the starting materials (**7a** + **11**) and the decarboxylation transition state [**1a**−**2a**]‡ (29.1 kcal mol^{-1}). For the *para*-case, the largest Gibbs energy span is between the starting materials (**7b** + **11**) and the transmetalation transition state [**25b**−**26b**]‡ (36.2 kcal mol^{-1}). This implies that for the *ortho*-case, the decarboxylation transition state and for the *para*-case, the transmetalation transition state is the rate-limiting transition state. Considering each step individually, one would come to a different conclusion since for the *ortho*-case, the barrier is lower in the decarboxylation (23.8 kcal mol^{-1}) compared to the transmetalation (24.9 kcal mol^{-1}), whereas for the *para*-case the barrier is higher in the decarboxylation (27.1 kcal mol^{-1}) than in the transmetalation (25.8 kcal mol^{-1}). This contrast stems from the exergonicity/endergonicity of the decarboxylation step as its products are the starting point for the subsequent transmetalation. For the *ortho*-case the decarboxylation is exergonic by −2.5 kcal mol^{-1} which decreases the starting point and the highest transition state of the transmetalation, while for the *para*-case the decarboxylation is endergonic by 5.4 kcal mol^{-1}, which increases the starting point and the highest transition state of the transmetalation, which explains the outcome of the overall reaction profile. For the *ortho*-case the difference between the heights of the decarboxylation (29.1 kcal mol^{-1}) and transmetalation transition state (27.7 kcal mol^{-1}) lies within the inaccuracy of the computational method. It is safe to say that the decarboxylation and the transmetalation are so similar in energy that it probably depends on the individual substrate which of these two steps will be rate-determining.

As discussed above, the reason for the high overall barrier of the transmetalation is the entropic penalty associated with forming an adduct of two species present only in catalytic amounts, together with a loss in solvation energy. The accuracy of some contributions to the activation energy such as solvent effects is difficult to assess. However, such systematic errors are likely to cancel out when calculating the *para*/*ortho* difference in the Gibbs energy span. This difference is considerable (7.1 kcal mol^{-1}), and agrees with the experimental observation that 4-fluorobenzoate is substantially less reactive than its *ortho*-isomer. Interestingly, the largest contribution to this difference stems from the exer-/endergonicity of the decarboxylation step, where the difference between *para* and *ortho* is $\Delta\Delta_r G_{sov} = 7.6$ kcal mol^{-1}.

Based on this profile, it can also be understood why the presence of halide anions can affect the reaction rate. The presence of excess bromide shifts the equilibrium of the anion exchange step to the side of the copper bromide so that less copper carboxylate is available. If for a given substrate the decarboxylation is the rate-determining step in a decarboxylative cross-coupling, the presence of excess bromide should have a similar effect, because it increases the energy span between **7** + **11** and [**1**−**2**]‡ + **10** by about 3 kcal mol^{-1}.

Experimental Studies. The above DFT studies suggest that the transmetalation is rate-limiting for substrates that decarboxylate comparatively easily. Bidentate ligands designed to bridge the two metals and bring them into close spatial proximity can be expected to facilitate this step. To test this hypothesis, we first searched for a benzoic acid that decarboxylates with particular ease. We performed a series of protodecarboxylation experiments in which various benzoic acids **22** were heated to 100 °C in the presence of 5 mol % Cu_2O and 10 mol % 1,10-phenanthroline (Table 1). No conversion was observed at this low temperature for most carboxylic acids tested, including 2- and 4-fluorobenzoic acid (**22a** or **22b**) (entries 1 and 2). However, 2-nitrobenzoic acid (**22c**) was smoothly converted into nitrobenzene (**30**) in near-quantitative yield (entry 5).

Table 1. Protodecarboxylation of Benzoic Acids[a]

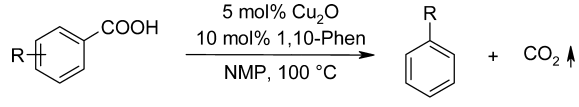

22 **23** or **30** **3**

entry	carboxylic acid	R	*t*/h	product	yield/%
1	**22a**	2-F	6	**23**	3
2	**22b**	4-F	6	**23**	0
3	**22c**	2-NO_2	6	**30**	64
4	**22d**	4-NO_2	6	**30**	0
5	**22c**	2-NO_2	24	**30**	99

[a]Reaction conditions: 0.5 mmol of carboxylic acid, 5 mol % Cu_2O, 10 mol % 1,10-Phen, 2.0 mL of NMP, 100 °C, GC yield after calibration.

It could thus be expected that the decarboxylation is not the rate-limiting step in a decarboxylative cross-coupling of 2-nitrobenzoic acid (**22c**) at 100 °C. We next performed various decarboxylative couplings at this temperature. Among all aryl electrophiles tested, triflates were the sole substrates to provide

dx.doi.org/10.1021/ja503295x | J. Am. Chem. Soc. 2014, 136, 10007−10023

Table 2. Decarboxylative Cross-Couplings with Monodentate and Bridging Ligands[a]

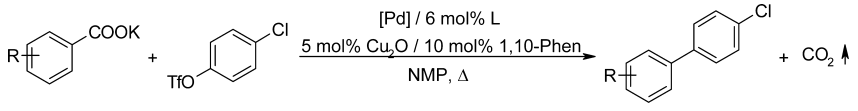

7 31 32 3

entry	carboxylate	R	temp/°C	L	product	yield/%
1	**7c**	2-NO_2	100	P(*p*-Tol)$_3$	**32c**	9
2	**7d**	4-NO_2	100	P(*p*-Tol)$_3$	**32d**	0
3[b]	**7c**	2-NO_2	170	P(*p*-Tol)$_3$	**32c**	84 (91)[7a]
4	**7c**	2-NO_2	100	L1	**32c**	0
5	**7c**	2-NO_2	100	L2	**32c**	0
6	**7c**	2-NO_2	100	L3	**32c**	0
7	**7c**	2-NO_2	100	L4	**32c**	40
8[c]	**7c**	2-NO_2	100	L4	**32c**	88

[a]Reaction conditions: 0.5 mmol of potassium carboxylate, 1 mmol of triflate, 5 mol % Cu_2O, 10 mol % 1,10-Phen, 2 mol % PdI_2, 6 mol % L, 2.0 mL of NMP, 100 °C, 24 h, GC yield after calibration. [b]1 mmol of potassium carboxylate, 2 mmol of triflate, 5 mol % Cu_2O, 10 mol % 1,10-Phen, 2 mol % PdI_2, 6 mol % P(*p*-Tol)$_3$, 4.0 mL of NMP, 170 °C, 1 h, GC yield after calibration, isolated yield in parentheses. [c]0.75 mmol of potassium carboxylate, 0.5 mmol of triflate, 5 mol % Cu_2O, 10 mol % 1,10-Phen, 3 mol % Pd(acac)$_2$, 6 mol % L4, 4.0 mL of NMP, 100 °C, 24 h, GC yield after calibration.

the coupling products in small amounts. For this reason, we investigated the coupling of 4-chlorophenyl triflate (**31**) with several potassium nitrobenzoates **7** as the model systems. With the best known catalyst system (Table 2), no conversion was observed in the coupling of potassium 4-nitrobenzoate (**7d**) with 4-chlorophenyl triflate (**31**) (entry 2), and potassium 2-nitrobenzoate (**7c**) gave less than 10% of 4-chloro-2′-nitrobiphenyl (**32c**) (entry 1). According to the literature, cross-couplings of aryl triflates with potassium benzoates with Cu/Pd systems and monodentate *p*-tolylphosphine have to be performed at 170 °C to give high yields.[7a,b]

We then replaced the *p*-tolylphosphine ligand by various bidentate P,N-ligands (Figure 9).[9,56] Among these, the

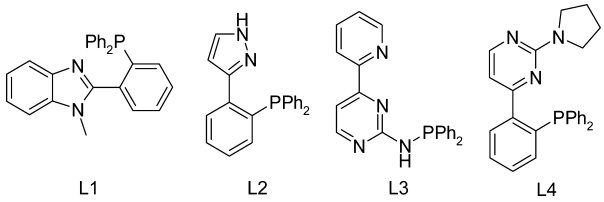

Figure 9. Bidentate P,N-ligands.

aminopyrimidinyl phosphines, especially ligand L4, developed by Thiel et al. in the context of other coupling reactions were most effective (entry 7).[56c] After slight modifications to the reaction conditions, the coupling product **32c** was detected in high yield (88%) already at 100 °C (entry 8).

Lowering the reaction temperature by as much as 70 °C is a decisive improvement over the state of the art, which we attribute to the ability of this ligand to bring copper and palladium into close proximity and thus assist the transmetalation step. The presence of bimetallic Cu−Pd complexes was confirmed by ESI-MS investigations of the reaction mixture, suggesting that their formation is no longer rate-determining.[28] Further experimental studies with the bidentate ligands, including the structural investigation of Cu/Pd adducts detected by ESI-MS, are underway. We are convinced that the concept of bringing the two metals together by bridging ligands will allow reaching new levels of efficiency in decarboxylative couplings of activated benzoates.

Conclusions and Outlook. The geometries and energies of all starting materials, products, intermediates, and transition states of the catalytic cycle were calculated for the decarboxylative cross-coupling of potassium 2- and 4-fluorobenzoate with bromobenzene in the presence of a catalyst system consisting of copper(I)/1,10-phenanthroline and the anionic monophosphine palladium complex [Pd(PMe$_3$)Br]$^-$. Among all pathways investigated, a catalytic cycle via neutral copper complexes was found to be most favorable. It consists of a carboxylate−bromide exchange at the copper center to give an uncharged copper carboxylate, followed by a decarboxylation step in which an organocopper species is generated. A palladium species that has been formed by oxidative addition of the aryl electrophile to a low-valent palladium(0) species accepts the aryl group from the copper in the subsequent transmetalation step, which links the catalytic cycles of the copper and palladium catalysts. The resulting diarylpalladium species undergoes reductive elimination, releasing the biaryl product and regenerating the palladium(0) species (Scheme 6).

Based on realistic assumptions on the inherent accuracy of these calculations, the energetic span model cannot unambiguously decide whether the decarboxylation or the transmetalation is rate-determining. This implies that depending on the substrate, either step can pose the main limitation in the catalyst performance. This is in sharp contrast to the current opinion that it is only the decarboxylation step that needs to be addressed in the catalyst improvement. The calculations also do not support the hypothesis that the difference in reactivity between *ortho*- and non-*ortho*-substituted carboxylates in the reaction with aryl halides is caused by the anion exchange step. The low reactivity of the latter is probably caused by the higher barrier of the decarboxylation process, which is further increased in relation to the starting material if excess halide salt is present.

In the transmetalation, the electronic activation energy is not overly high. It is the free energy loss in the initial adduct formation that makes it difficult. This result suggests that future research aimed at further improving the catalyst should also target the transmetalation and not only the decarboxylation step. This was confirmed by an experimental study, in which

dx.doi.org/10.1021/ja503295x | J. Am. Chem. Soc. 2014, 136, 10007−10023

the reaction temperature of a decarboxylative coupling was lowered by 70 °C by a P,N-ligand designed to facilitate adduct formation between copper and palladium. In combination with these experimental findings, the mechanistic studies presented herein are likely to induce a paradigm shift in the development of more active catalyst generations for decarboxylative cross-coupling reactions.

■ ASSOCIATED CONTENT

Supporting Information

Energies, graphical representations, geometrical parameters and Cartesian coordinates of all DFT-optimized structures. This material is available free of charge via the Internet at http://pubs.acs.org.

■ AUTHOR INFORMATION

Corresponding Author

goossen@chemie.uni-kl.de; vanwullen@chemie.uni-kl.de

Notes

The authors declare no competing financial interest.

■ ACKNOWLEDGMENTS

We thank W. R. Thiel for help with the DFT calculations and for providing P,N-ligands, K. Gooßen for help proofreading the manuscript, and M. F. Grünberg for technical assistance. We also thank the DFG (GO 853/5-2 and SFB-TRR 88 "3Met") and Landesgraduiertenförderung Rheinland-Pfalz (fellowship to A.F.) for funding.

■ REFERENCES

(1) (a) Nilsson, M. *Acta Chem. Scan.* **1966**, *20*, 423−426. (b) Nilsson, M.; Ullenius, C. *Acta Chem. Scand.* **1968**, *22*, 1998−2002. (c) Chodowska-Palicka, J.; Nilsson, M. *Acta Chem. Scand.* **1970**, *24*, 3353−3361. (d) Shimizu, I.; Yamada, T.; Tsuji, J. *Tetrahedron Lett.* **1980**, *21*, 3199−3202. (e) Tsuji, J.; Yamada, T.; Minami, I.; Yuhara, M.; Nisar, M.; Shimizu, I. *J. Org. Chem.* **1987**, *52*, 2988−2995. (f) Myers, A. G.; Tanaka, D.; Mannion, M. R. *J. Am. Chem. Soc.* **2002**, *124*, 11250−11251. (g) Tanaka, D.; Myers, A. G. *Org. Lett.* **2004**, *6*, 433−436. (h) Tanaka, D.; Romeril, S. P.; Myers, A. G. *J. Am. Chem. Soc.* **2005**, *127*, 10323−10333.

(2) Goossen, L. J.; Deng, G.; Levy, L. M. *Science* **2006**, *313*, 662−664.

(3) (a) Rudolphi, F.; Song, B.; Goossen, L. J. *Adv. Synth. Catal.* **2011**, *353*, 337−342. (b) Collet, F.; Song, B.; Rudolphi, F.; Goossen, L. J. *Eur. J. Org. Chem.* **2011**, 6486−6501.

(4) (a) Goossen, L. J.; Rudolphi, F.; Oppel, C.; Rodríguez, N. *Angew. Chem.* **2008**, *120*, 3085−3088; *Angew. Chem., Int. Ed.* **2008**, *47*, 3043−3045. (b) Grünberg, M. F.; Gooßen, L. J. *J. Organomet. Chem.* **2013**, *744*, 140−143.

(5) Goossen, L. J.; Rodríguez, N.; Melzer, B.; Linder, C.; Deng, G.; Levy, L. M. *J. Am. Chem. Soc.* **2007**, *129*, 4824−4833.

(6) Goossen, L. J.; Zimmermann, B.; Knauber, T. *Angew. Chem.* **2008**, *120*, 7211−7214; *Angew. Chem., Int. Ed.* **2008**, *47*, 7103−7106.

(7) (a) Goossen, L. J.; Rodriguez, N.; Linder, C. *J. Am. Chem. Soc.* **2008**, *130*, 15248−15249. (b) Goossen, L. J.; Linder, C.; Rodríguez, N.; Lange, P. P. *Chem.—Eur. J.* **2009**, *15*, 9336−9349. (c) Goossen, L. J.; Lange, P. P.; Rodríguez, N.; Linder, C. *Chem.—Eur. J.* **2010**, *16*, 3906−3909.

(8) Goossen, L. J.; Rodríguez, N.; Lange, P. P.; Linder, C. *Angew. Chem.* **2010**, *122*, 1129−1132; *Angew. Chem., Int. Ed.* **2010**, *49*, 1111−1114.

(9) Song, B.; Knauber, T.; Goossen, L. J. *Angew. Chem.* **2013**, *125*, 3026−3030; *Angew. Chem., Int. Ed.* **2013**, *52*, 2954−2958.

(10) Shang, R.; Fu, Y.; Wang, Y.; Xu, Q.; Yu, H. Z.; Liu, L. *Angew. Chem.* **2009**, *121*, 9514−9518; *Angew. Chem., Int. Ed.* **2009**, *48*, 9350−9354.

(11) Sun, Z. M.; Zhao, P. *Angew. Chem.* **2009**, *121*, 6854−6858; *Angew. Chem., Int. Ed.* **2009**, *48*, 6726−6730.

(12) Weaver, J. D.; Recio, A., III; Grenning, A. J.; Tunge, J. A. *Chem. Rev.* **2010**, *111*, 1846−1913.

(13) (a) Peschko, C.; Winklhofer, C.; Steglich, W. *Chem.—Eur. J.* **2000**, *6*, 1147−1152. (b) Forgione, P.; Brochu, M. C.; St-Onge, M.; Thesen, K. H.; Bailey, M. D.; Bilodeau, F. *J. Am. Chem. Soc.* **2006**, *128*, 11350−11351. (c) Bilodeau, F.; Brochu, M. C.; Guimond, N.; Thesen, K. H.; Forgione, P. *J. Org. Chem.* **2010**, *75*, 1550−1560. (d) Miyasaka, M.; Fukushima, A.; Satoh, T.; Hirano, K.; Miura, M. *Chem.—Eur. J.* **2009**, *15*, 3674−3677. (e) Miyasaka, M.; Hirano, K.; Satoh, T.; Miura, M. *Adv. Synth. Catal.* **2009**, *351*, 2683−2688. (f) Arroyave, F. A.; Reynolds, J. R. *Org. Lett.* **2010**, *12*, 1328−1331.

(14) (a) Moon, J.; Jeong, M.; Nam, H.; Ju, J.; Moon, J. H.; Jung, H. M.; Lee, S. *Org. Lett.* **2008**, *10*, 945−948. (b) Moon, J.; Jang, M.; Lee, S. *J. Org. Chem.* **2009**, *74*, 1403−1406. (c) Kima, H.; Lee, P. H. *Adv. Synth. Catal.* **2009**, *351*, 2827−2832. (d) Park, K.; Bae, G.; Moon, J.; Choe, J.; Song, K. H.; Lee, S. *J. Org. Chem.* **2010**, *75*, 6244−6251. (e) Zhang, W.-W.; Zhang, X.-G.; Li, J.-H. *J. Org. Chem.* **2010**, *75*, 5259−5264. (f) Zhao, D.; Gao, C.; Su, X.; He, Y.; You, J.; Xue, Y. *Chem. Commun.* **2010**, *46*, 9049−9051. (g) Park, K.; Bae, G.; Park, A.; Kim, Y.; Choe, J.; Song, K. H.; Lee, S. *Tetrahedron Lett.* **2011**, *52*, 576−580. (h) Park, A.; Park, K.; Kim, Y.; Lee, S. *Org. Lett.* **2011**, *5*, 944−947.

(15) Shang, R.; Fu, Y.; Li, J. B.; Zhang, S. L.; Guo, Q. X.; Liu, L. *J. Am. Chem. Soc.* **2009**, *131*, 5738−5739.

(16) Yin, L.; Kanai, M.; Shibasaki, M. *J. Am. Chem. Soc.* **2009**, *131*, 9610−9611.

(17) (a) Zhang, S. L.; Fu, Y.; Shang, R.; Guo, Q. X.; Liu, L. *J. Am. Chem. Soc.* **2010**, *132*, 638−646. (b) Hu, P.; Kan, J.; Su, W. P.; Hong, M. C. *Org. Lett.* **2009**, *11*, 2341−2344. (c) Fu, Z.; Huang, S.; Su, W.; Hong, M. *Org. Lett.* **2010**, *12*, 4992−4995. (d) Sun, Z.-M.; Zhang, J.; Zhao, P. *Org. Lett.* **2010**, *12*, 992−995. (e) Goossen, L. J.; Zimmermann, B.; Knauber, T. *Beilstein J. Org. Chem.* **2010**, *6*, 43−51.

(18) (a) Voutchkova, A.; Coplin, A.; Leadbeater, N. E.; Crabtree, R. H. *Chem. Commun.* **2008**, 6312−6314. (b) Wang, C. Y.; Piel, I.; Glorius, F. *J. Am. Chem. Soc.* **2009**, *131*, 4194−4195. (c) Cornella, J.; Lu, P.; Larrosa, I. *Org. Lett.* **2009**, *11*, 5506−5509. (d) Zhang, F.; Greaney, M. F. *Angew. Chem.* **2010**, *122*, 2828−2831; *Angew. Chem., Int. Ed.* **2010**, *49*, 2768−2771.

(19) (a) Gledhill, A. P.; McCall, C. J.; Threadgill, M. D. *J. Org. Chem.* **1986**, *51*, 3196−3201. (b) Huang, W. H.; Wang, M. L.; Yue, H. *Synthesis* **2008**, 1342−1344. (c) Bi, H.-P.; Zhao, L.; Liang, Y.-M.; Li, C.-J. *Angew. Chem.* **2009**, *121*, 806−809; *Angew. Chem., Int. Ed.* **2009**, *48*, 792−795. (d) Bi, H.-P.; Chen, W.-W.; Liang, Y.-M.; Li, C.-J. *Org. Lett.* **2009**, *11*, 3246−3249.

(20) (a) Duan, Z. Y.; Ranjit, S.; Zhang, P. F.; Liu, X. G. *Chem.—Eur. J.* **2009**, *15*, 3666−3669. (b) Jia, W.; Jiao, N. *Org. Lett.* **2010**, *12*, 2000−2003. (c) Ranjit, S.; Duan, Z.; Zhang, P.; Liu, X. *Org. Lett.* **2010**, *12*, 4134−4136.

(21) (a) President's Information Technology Advisory Committee. *Computational Science: Ensuring America's Competitiveness*; Arlington, VA, 2005. (b) Mpourmpakis, G.; Vlachos, D. G. *MRS Bull.* **2011**, *36*, 211−215. and references therein (c) Goossen, L. J.; Rodríguez, N.; Linder, C.; Lange, P. P.; Fromm, A. *ChemCatChem.* **2010**, *2*, 430−442. (d) Dudnik, A. S.; Xia, Y.; Li, Y.; Gevorgyan, V. *J. Am. Chem. Soc.* **2010**, *132*, 7645−7655.

(22) Goossen, L. J.; Thiel, W. R.; Rodríguez, N.; Linder, C.; Melzer, B. *Adv. Synth. Catal.* **2007**, *349*, 2241−2246.

(23) (a) Braga, A. A. C.; Ujaque, G.; Maseras, F. *Organometallics* **2006**, *25*, 3647−3658. and references therein (b) Kozuch, S.; Shaik, S.; Jutand, A.; Amatore, C. *Chem.—Eur. J.* **2004**, *10*, 3072−3080. (c) Kozuch, S.; Amatore, C.; Jutand, A.; Shaik, S. *Organometallics* **2005**, *24*, 2319−2330.

(24) (a) Goossen, L. J.; Koley, D.; Hermann, H.; Thiel, W. *J. Am. Chem. Soc.* **2005**, *127*, 11102−11114. (b) Goossen, L. J.; Koley, D.; Hermann, H.; Thiel, W. *Organometallics* **2006**, *25*, 54−67.

(25) Keith, J. A.; Behenna, D. C.; Mohr, J. T.; Ma, S.; Marinescu, S. C.; Oxgaard, J.; Stoltz, B. M.; Goddard, W. A., III *J. Am. Chem. Soc.* **2007**, *129*, 11876−11877.
(26) Shang, R.; Xu, Q.; Jiang, Y.-Y.; Wang, Y.; Liu, L. *Org. Lett.* **2010**, *12*, 1000−1003.
(27) Xie, H.; Lin, F.; Lei, Q.; Fang, W. *Organometallics* **2013**, *32*, 6957−6968.
(28) Hackenberger, D.; Song, B.; Grünberg, M. F.; Farsadpour, S.; Taghizadeh Ghoochany, L.; Menges, F.; Burkhardt, L.; Niedner-Schatteburg, G.; Thiel, W. R.; Goossen, L. J., *unpublished results*.
(29) Recently, related studies have investigated the transfer of an aryl group from palladium to gold: Perez-Temprano, M. H.; Casares, J. A.; de Lera, A. R.; Alvarez, R.; Espinet, P. *Angew. Chem., Int. Ed.* **2012**, *51*, 4917−4920.
(30) (a) *Gaussian 03*, Revision E.01; Gaussian, Inc.: Wallingford, CT, 2004. (b) *Gaussian 09*, Revision D.01; Gaussian, Inc.: Wallingford, CT, 2013; for full citations see the Supporting Information.
(31) (a) Stephens, P. J.; Devlin, F. J.; Chabalowski, C. F.; Frisch, M. J. *J. Phys. Chem.* **1994**, *98*, 11623−11627. (b) Becke, A. D. *J. Chem. Phys.* **1993**, *98*, 5648−5652. (c) Becke, A. D. *Phys. Rev. A* **1988**, *38*, 3098−3100. (d) Lee, C.; Yang, W.; Parr, R. G. *Phys. Rev. B* **1988**, *37*, 785−789.
(32) (a) Ditchfield, R.; Hehre, W. J.; Pople, J. A. *J. Chem. Phys.* **1971**, *54*, 724−728. (b) Hehre, W. J.; Ditchfield, R.; Pople, J. A. *J. Chem. Phys.* **1972**, *56*, 2257−2261. (c) Hariharan, P. C.; Pople, J. A. *Theor. Chim. Acta* **1973**, *28*, 213−222. (d) Clark, T.; Chandrasekhar, J.; Spitznagel, G. W.; Schleyer, P. v. R. *J. Comput. Chem.* **1983**, *4*, 294−301. (e) Rassolov, V. A.; Pople, J. A.; Ratner, M. A.; Windus, T. L. *J. Chem. Phys.* **1998**, *109*, 1223−1229. (f) Binning, R. C., Jr.; Curtiss, L. A. *J. Comput. Chem.* **1990**, *11*, 1206−1216. (g) Dunning, T. H. *J. Chem. Phys.* **1977**, *66*, 1382−1383.
(33) (a) Dolg, M.; Wedig, U.; Stoll, H.; Preuss, H. *J. Chem. Phys.* **1987**, *86*, 866−872. (b) Andrae, D.; Häußermann, U.; Dolg, M.; Stoll, H.; Preuss, H. *Theor. Chim. Acta* **1990**, *77*, 123−141.
(34) (a) Peng, C.; Schlegel, H. B. *Isr. J. Chem.* **1994**, *33*, 449−454. (b) Peng, C.; Ayala, P. Y.; Schlegel, H. B.; Frisch, M. J. *J. Comput. Chem.* **1996**, *17*, 49−56.
(35) (a) Fukui, K. *Acc. Chem. Res.* **1981**, *14*, 363−368. (b) Hratchian, H. P.; Schlegel, H. B. In *Theory and Applications of Computational Chemistry: The First 40 Years*; Dykstra, C. E., Frenking, G., Kim, K. S., Scuseria, G., Eds.; Elsevier: Amsterdam, The Netherlands, 2005; pp 195−249. (c) Hratchian, H. P.; Schlegel, H. B. *J. Chem. Phys.* **2004**, *120*, 9918−9924. (d) Hratchian, H. P.; Schlegel, H. B. *J. Chem. Theory Comput.* **2005**, *1*, 61−69.
(36) (a) Krishnan, R.; Binkley, J. S.; Seeger, R.; Pople, J. A. *J. Chem. Phys.* **1980**, *72*, 650−654. (b) Curtiss, L. A.; McGrath, M. P.; Blaudeau, J.-P.; Davis, N. E.; Binning, R. C.; Radom, L. *J. Chem. Phys.* **1995**, *103*, 6104−6113. (c) Blaudeau, J.-P.; McGrath, M. P.; Curtiss, L. A.; Radom, L. *J. Chem. Phys.* **1997**, *107*, 5016−5021.
(37) Weigend, F.; Ahlrichs, R. *Phys. Chem. Chem. Phys.* **2005**, *7*, 3297−3305.
(38) (a) Barone, V.; Cossi, M. *J. Phys. Chem. A* **1998**, *102*, 1995−2001. (b) Cossi, M.; Rega, N.; Scalmani, G.; Barone, V. *J. Comput. Chem.* **2003**, *24*, 669−681.
(39) (a) Klamt, A.; Schüürmann, G. *J. Chem. Soc., Perkin Trans. 2* **1993**, 799−805. (b) Schäfer, A.; Klamt, A.; Sattel, D.; Lohrenz, J. C. W.; Eckert, F. *Phys. Chem. Chem. Phys.* **2000**, *2*, 2187−2193.
(40) Wong, M. W. *Chem. Phys. Lett.* **1996**, *256*, 391−399.
(41) Murrieta-Guevara, F.; Romero-Martinez, A.; Trejo, A. *Fluid Phase Equilib.* **1988**, *44*, 105−115.
(42) Johnson, E. R.; Mackie, I. D.; DiLabio, G. A. *J. Phys. Org. Chem.* **2009**, *22*, 1127−1135.
(43) Grimme, S.; Antony, J.; Ehrlich, S.; Krieg, H. *J. Chem. Phys.* **2010**, *132*, 154104.
(44) Riley, K. E.; Vondrasek, J.; Hobza, P. *Phys. Chem. Chem. Phys.* **2007**, *9*, 5555−5560.
(45) *GaussView 5.0.8*; Gaussian, Inc.: Wallingford, CT, 2008.
(46) See the Supporting Information for details.
(47) (a) Goossen, L. J.; Koley, D.; Hermann, H.; Thiel, W. *Chem. Commun.* **2004**, 2141−2143. (b) Goossen, L. J.; Koley, D.; Hermann, H.; Thiel, W. *Organometallics* **2005**, *24*, 2398−2410.
(48) Hammond, G. S. *J. Am. Chem. Soc.* **1955**, *77*, 334−338.
(49) Bondi, A. *J. Phys. Chem.* **1964**, *68*, 441−451.
(50) Ebihara, M.; Tokoro, K.; Maeda, M.; Ogami, M.; Imaeda, K.; Sakurai, K.; Masuda, H.; Kawamura, T. *J. Chem. Soc., Dalton Trans.* **1994**, 3621−3635.
(51) Liu, I. P.-C.; Lee, G.-H.; Peng, S.-M.; Bénard, M.; Rohmer, M.-M. *Inorg. Chem.* **2007**, *46*, 9602−9608.
(52) Maynau, D.; Bolvin, H.; Van den Heuvel, W.; Bénard, M.; Rohmer, M.-M.; Ben Amor, N. *C. R. Chim.* **2012**, *15*, 170−175.
(53) Tanabe, M.; Ishikawa, N.; Chiba, M.; Ide, T.; Osakada, K.; Tanase, T. *J. Am. Chem. Soc.* **2011**, *133*, 18598−18601.
(54) Amatore, C.; Jutand, A. *J. Organomet. Chem.* **1999**, *576*, 254−278.
(55) Kozuch, S.; Shaik, S. *Acc. Chem. Res.* **2011**, *44*, 101−110.
(56) (a) Sun, Y.; Hienzsch, A.; Grasser, J.; Herdtweck, E.; Thiel, W. R. *J. Organomet. Chem.* **2006**, *691*, 291−298. (b) Sarcher, C.; Farsadpour, S.; Taghizadeh Ghoochany, L.; Sun, Y.; Thiel, W. R.; Roesky, P. W. *Dalton Trans.* **2014**, *43*, 2397−2405. (c) Farsadpour, S.; Taghizadeh Ghoochany, L.; Sun, Y.; Thiel, W. R. *Eur. J. Inorg. Chem.* **2011**, *29*, 4603−4609.